(4)

ASSESSMENT OF A NOVEL RF LINAC AMPLIFIER CONCEPT

Science Applications International Corporation

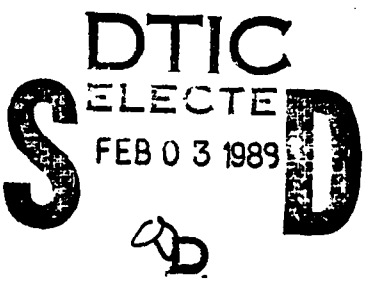

88 10 4 099

ASSESSMENT OF A NOVEL RF LINAC AMPLIFIER CONCEPT

By

S. A. Mani, L. Kahan, and A. Dudkin

FINAL REPORT

20 September 1988

Prepared for

Office of Naval Research
800 No. Quincy Street
Arlington, VA 22217-5000

Under Contract No. N00014-87-C-0230

SCIENCE APPLICATIONS INTERNATIONAL CORPORATION
1040 Waltham Street
Lexington, MA 02173-8027
(617) 863-5173

UNCLASSIFIED

SECURITY CLASSIFICATION OF THIS PAGE

REPORT DOCUMENTATION PAGE

Form Approved
OMB No 0704-0188
Exp Date Jun 30, 1986

1a. REPORT SECURITY CLASSIFICATION
Unclassified

1b. RESTRICTIVE MARKINGS

2. SECURITY CLASSIFICATION AUTHORITY

3. DISTRIBUTION/AVAILABILITY OF REPORT

2b. DECLASSIFICATION/DOWNGRADING SCHEDULE

4. PERFORMING ORGANIZATION REPORT NUMBER(S)
SAIC 88/1869

5. MONITORING ORGANIZATION REPORT NUMBER(S)

6a. NAME OF PERFORMING ORGANIZATION
Science Applications International Corporation

6b. OFFICE SYMBOL (If applicable)

7a. NAME OF MONITORING ORGANIZATION
Office of Naval Research

6c. ADDRESS (City, State, and ZIP Code)
1040 Waltham Street
Lexington, MA 02173-8027

7b. ADDRESS (City, State, and ZIP Code)
Naval Ocean Systems Center
ATTN: Dr. Vern Smiley, Code 54
271 Catalina Blvd, San Diego, CA 92152-5000

8a. NAME OF FUNDING/SPONSORING ORGANIZATION
Office of Naval Research

8b. OFFICE SYMBOL (If applicable)

9. PROCUREMENT INSTRUMENT IDENTIFICATION NUMBER

8c. ADDRESS (City, State, and ZIP Code)
800 No. Quincy Street
Arlington, VA 22217-5000

10. SOURCE OF FUNDING NUMBERS

PROGRAM ELEMENT NO.	PROJECT NO.	TASK NO.	WORK UNIT ACCESSION NO.

11. TITLE (Include Security Classification)
ASSESSMENT OF A NOVEL RF LINAC AMPLIFIER CONCEPT

12. PERSONAL AUTHOR(S)
Siva A. Mani, Lloyd Kahan, and Andrey Dudkin

13a. TYPE OF REPORT	13b. TIME COVERED	14. DATE OF REPORT (Year, Month, Day)	15. PAGE COUNT
Final	FROM 6/87 TO 7/88	1988/09/20	53

16. SUPPLEMENTARY NOTATION

17. COSATI CODES		
FIELD	GROUP	SUB-GROUP

18. SUBJECT TERMS (Continue on reverse if necessary and identify by block number)
FEL, BEAM COMBINER, RF LINAC, STIMULATED ROTATIONAL RAMAN AMPLIFIER, SCATTERING, SRRS

19. ABSTRACT (Continue on reverse if necessary and identify by block number)

Free Electron Laser

In this report, we discuss a potential method of increasing the peak current of an rf linear accelerator without significantly degrading the transverse emittance of the beam. This can be achieved at the expense of increasing the longitudinal phase space of the beam; if this increase in longitudinal phase space is acceptable, the FEL performance does not degrade much. First, we describe our concept for increasing the micropulse peak current. We then estimate the change in brightness of the beam using first order transport properties of the beam. We have also analyzed the performance of the FEL amplifier for different electron and optical beam parameters using a one-dimensional code. The advantages of increasing the peak current are clearly shown. Finally, we present the results of our analysis on the transient stimulated Raman scattering analysis and its effect on both up and down links. Keywords: Electron-beams, Laser amplifiers. (RH/F.I.)

20. DISTRIBUTION/AVAILABILITY OF ABSTRACT
☒ UNCLASSIFIED/UNLIMITED ☐ SAME AS RPT. ☐ DTIC USERS

21. ABSTRACT SECURITY CLASSIFICATION
Unclassified

22a. NAME OF RESPONSIBLE INDIVIDUAL
Siva A. Mani

22b. TELEPHONE (Include Area Code)
(617) 863-5173

22c. OFFICE SYMBOL

DD FORM 1473, 84 MAR 83 APR edition may be used until exhausted. SECURITY CLASSIFICATION OF THIS PAGE

TABLE OF CONTENTS

LIST OF FIGURES

ACKNOWLEDGEMENTS

The authors would like to thank Roger Kennedy of the Boeing Aircraft Company and Phil Morton and Karl Brown of the Stanford Linear Accelerator Center for helpful discussions on the beam combiner and for help running the transport code.

I. INTRODUCTION

The free electron laser converts the kinetic energy of a relativistic electron beam into a coherent electromagnetic field through the combined action of a transverse wiggler field and the electromagnetic field. For scaling the free electron laser to very high average powers, it is necessary to operate the laser in a Master Oscillator - Power Amplifier (MOPA) configuration. The two most important sources of high energy electron beams suitable for use in the FEL are the rf linear accelerator and the induction linear accelerator. The rf linear accelerator technology is mature and the linac is capable of producing beams with peak currents of a few hundred amperes sufficient for sustaining oscillation in a resonator. In addition, the electron beam brightness from the rf linear accelerator is at least an order of magnitude greater than what is required for successful FEL operation. Moreover, the optical output obtained from an rf linac FEL consists of extremely short micropulses that enable the laser beam to propagate through the atmosphere without stimulated rotational Raman scattering (SRRS) by N_2. This particular feature has important implications for the BMD missions for which the free electron lasers are being seriously considered. However, for successful amplifier operation with sufficiently high gain (>15 dB) and high extraction efficiency (>20%), it is desirable that the peak current of the accelerator be in the 1 kAmp or greater range.

In this report, we discuss a potential method to increase the peak current of a rf linear accelerator without significantly degrading the transverse emittance of the beam. This can be achieved at the expense of increasing the longitudinal phase space of the beam; if this increase in longitudinal phase space is acceptable, the FEL performance does not degrade much. In the next section we describe our concept for increasing the micropulse peak current.

We then estimate the change in brightness of the beam using first order transport properties of the beam. In Section III, we anlayze the performance of the FEL amplifier for different electron and optical beam parameters. Section IV describes our results of transient stimulated Raman scattering analysis and its effect on both up and down links. Section V summarizes our findings and makes recommendations for future work.

II. ANALYSIS OF BEAM COMBINER

Current rf linac technology can provide micropulse peak currents of up to 500 amperes at a brightness of $> 10^{11}$ amp/(m-rad)^2. For amplifier operation, a threshold current or ~2 kamp at a brightness of 10^9 amp/(m-rad)^2 is typically required. At higher brightnesses interesting FEL performances can be achieved at lower threshold currents. In what follows, we shall illustrate how two micropulses can be combined to give twice the current at twice or slightly less than twice the brightness. The concept can be extended in a straightforward manner to combining more than two pulses.

There are several schemes for combining the micropulses. The easiest way would be to combine the micropulses from several near identical linacs using "CHICANE". This technique is well known to accelerator physicists. What this requires is slight energy difference between the different accelerator micropulses. The CHICANE works essentially as an electron spectrometer in reverse. In the electron spectrometer, particles of different kinetic energies are bent through different angles in a transverse magnetic field and thus can be separated. If the particle motions are reversed, electrons starting from different spatial positions with differing energies can be combined to form a single pulse. The price that one pays for increasing the current in the above manner is that the energy spread of the beam is increased. If the increased energy spread is acceptable to the FEL, the concept has some merit. If one wants to reduce the accelerator hardware and use only a single accelerator, one could combine adjacent micropulses by the following technique. At the end of the linac add an rf cavity operating at a frequency such that the successive micropulses enter this last cavity out of phase. Thus if the first micropulse gains energy in this last cavity, the 2nd and 4th, 6th, ..., 2Nth pulses will lose energy while all odd pulses will gain

energy. This is illustrated in Fig. 2.1. Clearly if the frequency of this last cavity is one half of the fundamental frequency of the linac, one can introduce energy spread between successive micropulses.

Other frequencies of operation for this linac are also possible. Let f be the fundamental cavity frequency of the accelerator prior to the final cavity and let ν be the frequency of the cavity that imparts the energy dispersion to the different micropulses. If the harmonic number of the bunches is h, then the interpulse duration T_p is equal to h/f. The RF phase between the successive micropulses in the final cavity is then equal to $2\pi\nu T_p$. Setting this equal to $(2n+1)\pi$, where n is an integer, we find that

$$\nu = (n + \frac{1}{2})f/h \qquad (2.1)$$

Choosing n to be equal to h or h-1, we get a frequency for the final cavity to be close to the accelerator frequency f. For example, if f = 500 MHz and h = 5, we see that ν = 500 ±50 MHz would make every other micropulse to have a slightly larger energy than the ones interleaving them. It is, of course, not necessary to choose n to be equal to h or h-1; it is only a convenient way of sizing the cavity.

Once the adjacent micropulses are separated in energy, it is a simple matter to separate them spatially with a dipole magnetic field. The two bunches then are made to transverse through different isochronous and achromatic transport systems. The transport systems are chosen such that one bunch travels an additional distance = $h\beta c/f$, where c is the speed of light, and $\beta = v/c \approx 1$. These two transport systems bring the two bunches close to each other to positions which are identical to the ones at the start of the transport systems (at least to the first order). The two bunches then can be combined to form a single bunch by reversing the process which separated them

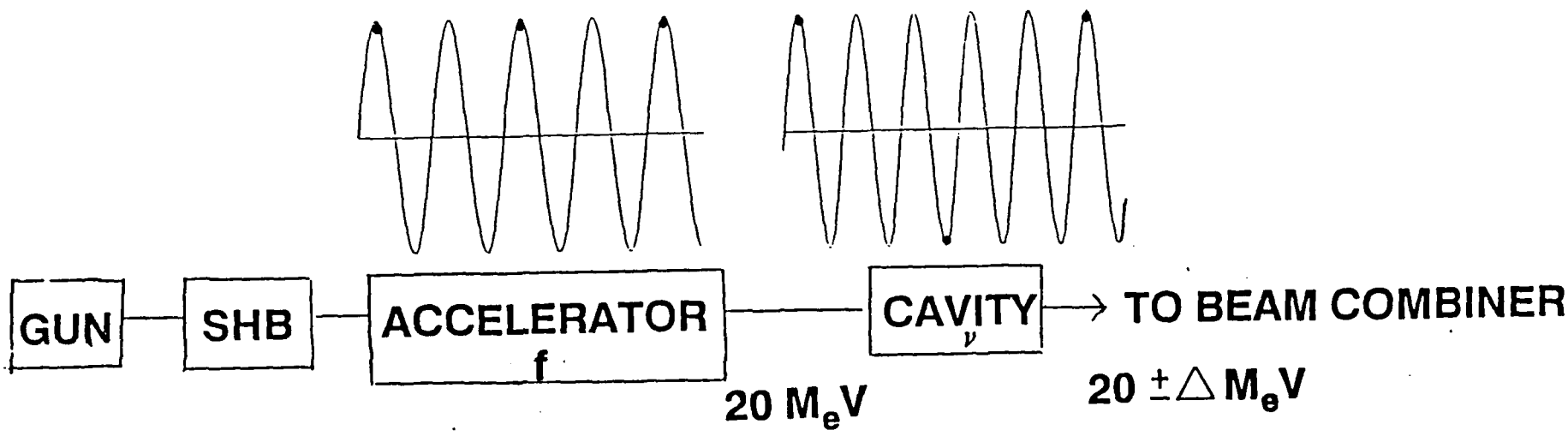

FIG. 2.1 - SCHEMATIC OF THE ACCELERATOR CAVITIES SHOWING ENERGY ADDITION TO SELECTED MICROPULSES. BLACK DOTS REPRESENT THE POSITION OF MICROPULSES WITH RESPECT TO THE RF WAVE.

spatially in the first place. The schematic of one such beam combiner is shown in Fig. 2.2. The beam combiner therefore can be separated into four components. The first is the accelerator cavity tuned to the frequency ν to provide energy dispersion between adjacent micropulses; the second is the magnetic deflection system that separates adjacent micropulses spatially; the third is the isochronous and achromatic transport system that has different path lengths to bring the two beams to coincidence temporally; the last is the deflection system to bring the two bunches together spatially. This last component is the mirror image of the second component. Once the adjacent beams are brought together, they can be accelerated further in cavities tuned to the frequency f. This will reduce the effective energy spread in the beam. For example, if the FEL is designed to operate at 200 MeV, then the beam combiner can be made to operate as 20±1 MeV. The 2 MeV energy spread imparted by the beam combiner amounts to only 1% of the final energy and it may be within the energy acceptance of the tapered wiggler amplifier.

For the magnetic deflector we choose a system first proposed and analyzed by Penner.[1] He analyzed a three-magnet system for nondispersive deflection of a nearly parallel beam. Figure 2.3 shows such a system. The curve with arrows represents the central trajectory. The symmetry axis is SS. Electrons which are initially parallel at the entrance phase JJ get dispersed at SS if they are of different energy and they become parallel again at the exit plane OO so if we break the deflection system at SS, we should be able to spatially separate the two adjacent micropulses which have different energy. Each pulse then is transported through achromatic and isochronous transports to the S′S′ plane where the beam properties are identical to what they were at SS. The difference between the two transport systems is that one of them has extra path length which is chosen to be equal to the inter-pulse distance. The

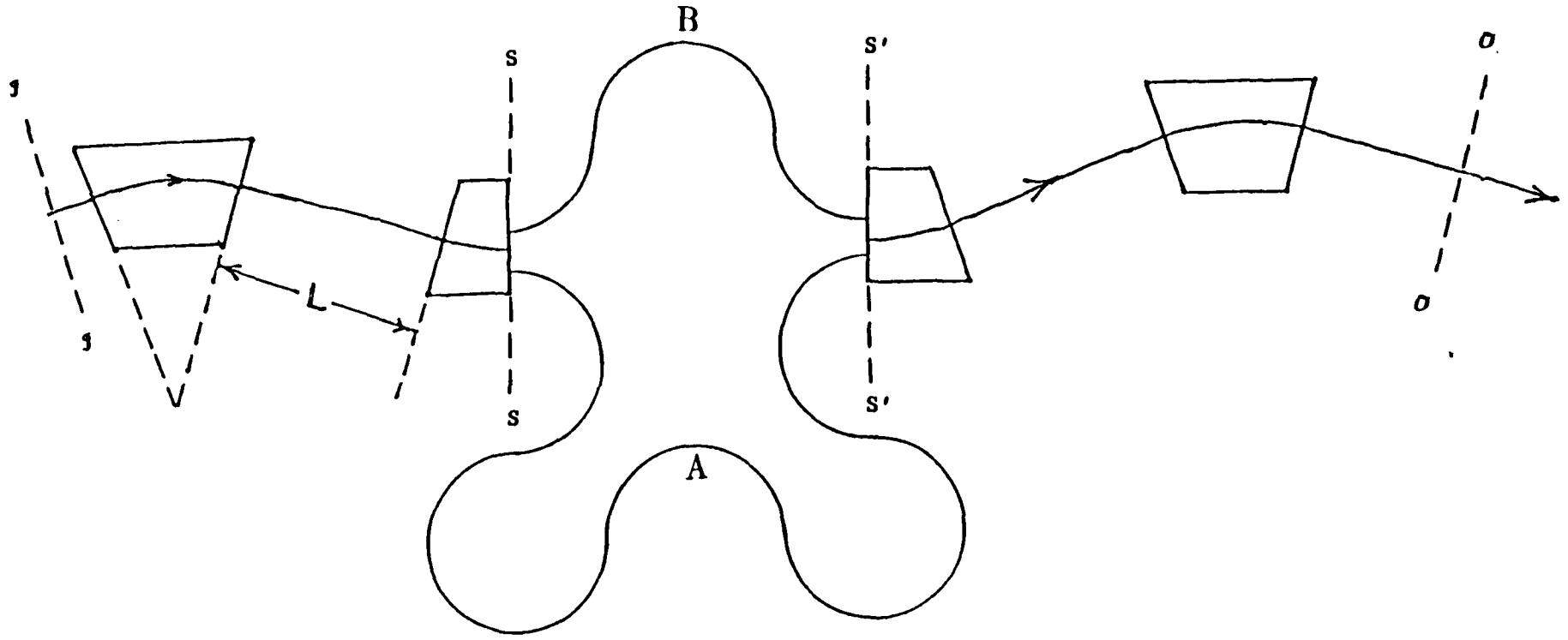

FIG. 2.2 - SCHEMATIC OF THE TRANSPORT OPTICS FOR THE BEAM COMBINER

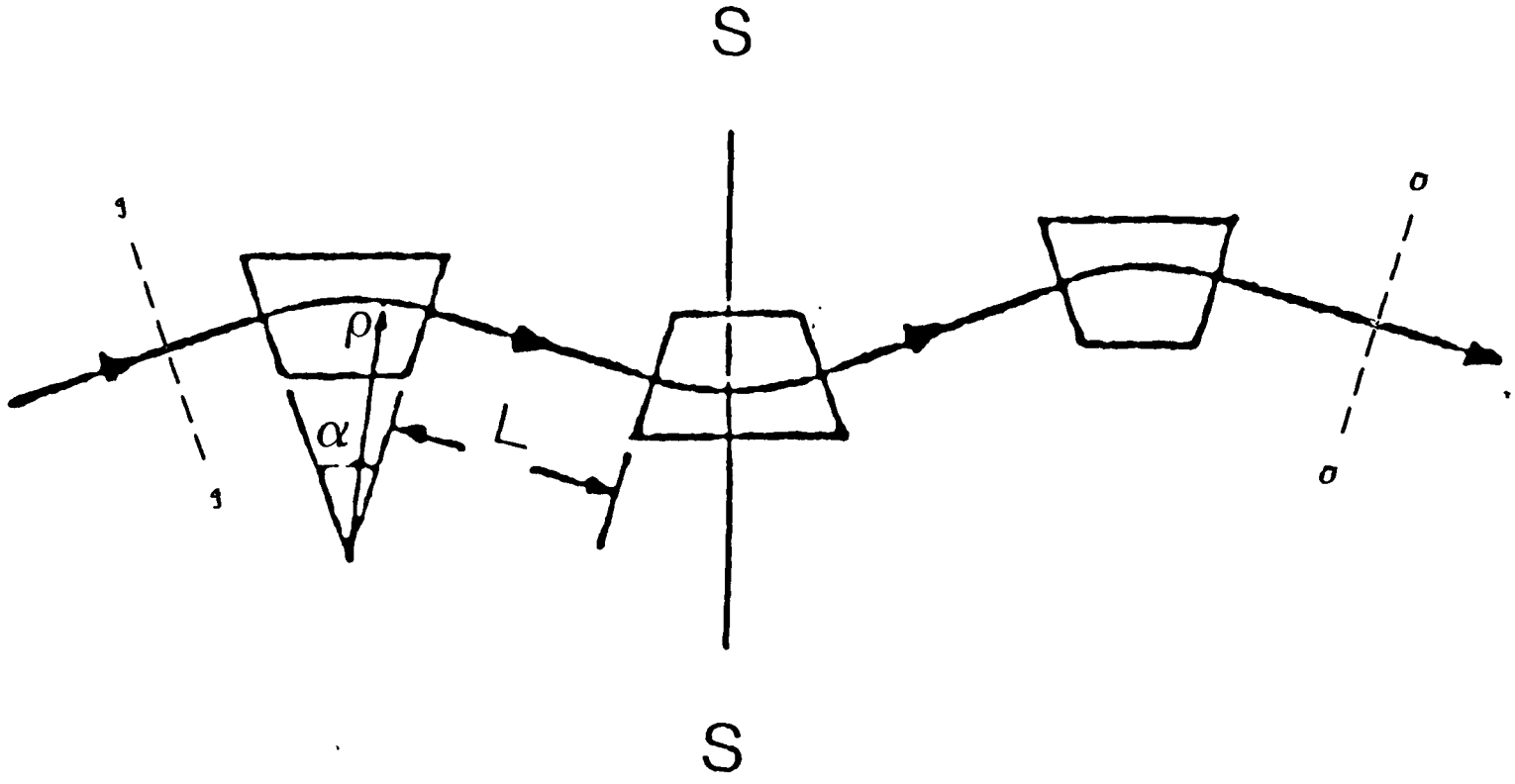

FIG. 2.3 - THREE MAGNET SYSTEM FOR NONDISPERSIVE DEFLECTION

final section of the beam combiner is the same as the component between SS and OO in Fig. 2.3.

We use matrix methods for analyzing the properties of the magnet systems. Matrix methods for calculating trajectories are well known in optics[2] and have been applied to electron optics.[3,4,5] In the matrix theory, the position and direction of travel of a particle entering a beam line is represented via a vector with six coordinates[6]

$$\mathbf{X} = \begin{bmatrix} x \\ x' \\ y \\ y' \\ \ell \\ \delta \end{bmatrix} \tag{2.2}$$

The coordinates x and y represent, respectively, the horizontal and vertical displacements at the position of the particle, and x' and y' represent the angles with the axis of the beam line in the same planes. The quantity ℓ represents the longitudinal position of the particle relative to a particle traveling on the magnetic axis of the system with the central momentum designed for the system. The remaining quantity $\delta = (p - p_o)/p_o$ gives the fractional deviation of the momentum of the particle from the central design momentum of the system.

The effect of the passage of a particle across a magnetic element or a drift space is represented to the first order by a transfer matrix R. The coordinates $\mathbf{X}_1$ of the particle at the end of the element are then given in terms of those at the beginning $\mathbf{X}_o$ as

$$\mathbf{X}_1 = \mathbf{R}\,\mathbf{X}_o \tag{2.3}$$

The effect of successive elements, each with its own R matrix is given by a total R matrix R(t) which is equal to the product of the individual R matrices.

$$R(t) = R_n R_{n-1} \ldots R_2 R_1 \tag{2.4}$$

The transfer matrix R is a 6 x 6 matrix and the problem of designing the beam combiner reduces to (a) finding the R matrices for the different elements and (b) finding a suitable coordination of the R matrices that give the desired total R matrix. In our case, we would like R(t) for the beam combining to be as close to a unit matrix as possible.

Second order corrections and the effect of deviation from the nominal design on the system performance may then be applied. If all the bends and focussing are carried out in a single plane, we can work with a reduced 4 x 4 R matrix to make a preliminary design calculation. This will be the approach that we take in this report. The X vector in this case will have only four coordinates x, x', ℓ and δ.

For the dispersive section $\mathcal{JJ}$-SS, the transfer matrix R_1 is given by

$$R_1 = \begin{bmatrix} 0 & \rho/2\sin\beta & 0 & \rho(2\cos\beta-1) \\ -2\sin\beta/\rho & (4\cos\beta-3\sec\beta)/2 & 0 & 0 \\ 2\sin\beta(2\cos\beta-1) & \rho(1-2\cos\alpha+2\cos\beta-1.5\sec\beta) & 1 & \rho(3\beta-2\sin\alpha) \\ 0 & 0 & 0 & 1 \end{bmatrix} \tag{2.5}$$

where α is the magnet bend angle, $\beta = \alpha/2$ and ρ is the radius of curvature of t. e central trajectory.[1]

The transfer matrix between SS and S'S' should be designed to be unity. What this means is that the transport system be achromatic and isochronous. Achromaticity can be easily achieved by demanding that the total phase shift between entrance and exit be an integral multiple of 2π radians. A little digression may be necessary to explain this point. A particle which deviates from the central trajectory executes betatron oscillations around the central trajectory. To first order, the period of this oscillation depends only on the central momentum and magnet parameters. So if the transport system is designed such that the total length equal to the wavelength of the oscillation, all particles will end up with the same x and x' coordinates as they started with. Thus the transport system will be automaticaly achromatic. However, particles with different energy may take different path lengths through the transport. So the system may not be isochronous. Elements with negative dispersion (momentum compaction) may be added to cancel any positive dispersion present in the system. We have chosen the transport between SS and S'S' to be synthesized from elements comprising 90° deflection system as shown in Fig. 2.4. The transfer matrices for this system can be written as

$$R_d^+ = \begin{bmatrix} -1 & 2\rho(\sqrt{2} - 1) & 0 & 0 \\ 0 & -1 & 0 & 0 \\ \sqrt{2} & \rho(2 - \sqrt{2}) & 1 & 0 \\ 0 & 0 & 0 & 1 \end{bmatrix} \tag{2.6}$$

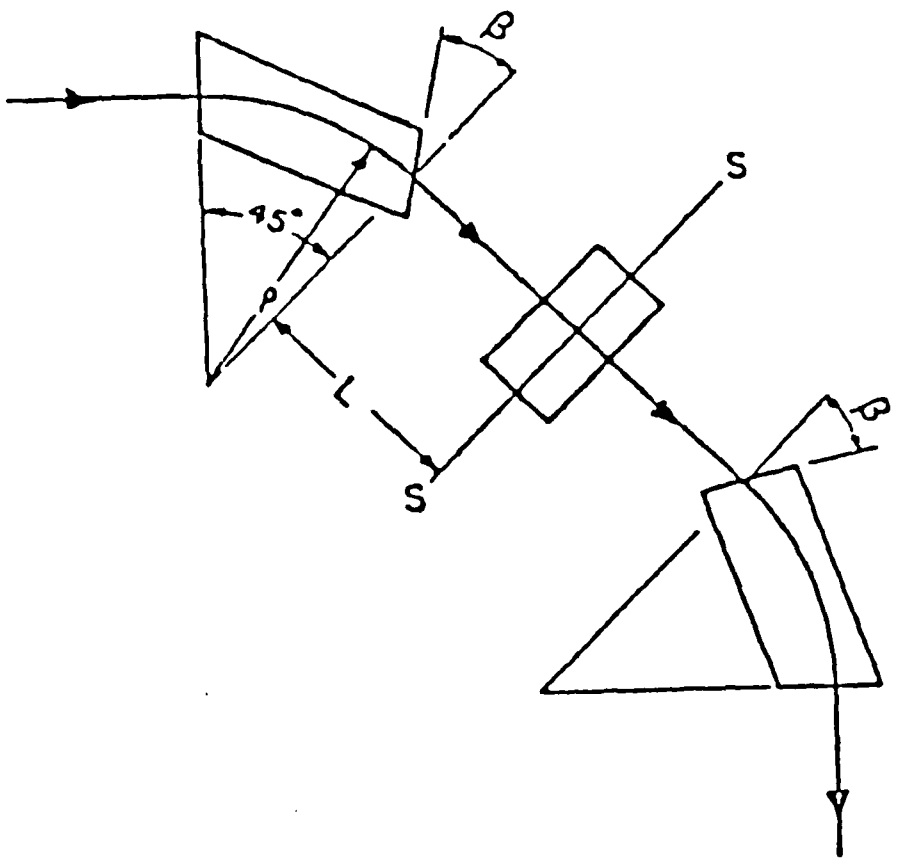

FIG. 2.4 - MAGNET SYSTEM FOR NONDISPERSIVE 90° DEFLECTION

$$R_d^- = \begin{bmatrix} -1 & 2\rho(\sqrt{2}-1) & 0 & 0 \\ 0 & -1 & 0 & 0 \\ -\sqrt{2} & -\rho(2-\sqrt{2}) & 1 & 0 \\ 0 & 0 & 0 & 1 \end{bmatrix} \tag{2.7}$$

where the superscripts + and - denote whether the bend is to the right or left respectively of the central trajectory at the entrance.

The transfer matrix for path A can be written as

$$R_d^+ R_d^+ R_d^- R_d^- R_d^- R_d^+ R_d^+ R_d^- R_d^- R_d^- R_d^+ R_d^+ = I \tag{2.8}$$

where I is the identity matrix. Similarly, the transfer matrix for path B can be written as

$$R_d^- R_d^+ R_d^+ R_d^- = I \tag{2.9}$$

The validity of Eqs. (2.8) and (2.9) can be readily seen by direct multiplication using Eqs. (2.6) and (2.7). If Eq. (2.9) is true, it is easy to show that Eq. (2.8) must be true as follows:

$$R_d^+ R_d^+ R_d^- R_d^- R_d^- R_d^+ R_d^+ R_d^- R_d^- R_d^- R_d^+ R_d^+$$

$$= R_d^+ R_d^+ R_d^- R_d^- \cdot R_d^+ R_d^- R_d^- R_d^+ \cdot R_d^- R_d^- R_d^+ R_d^+$$

$$= R_d^+ (R_d^+ R_d^- R_d^- R_d^+) R_d^- R_d^- (R_d^+ R_d^- R_d^- R_d^+) R_d^+$$

$$= R_d^+ R_d^- R_d^- R_d^+ = I \tag{2.10}$$

The trick was to interchange the + and - signs in the middle four elements of Eq. (2.8) since they multiply out to identity matrix. The rest follows naturally by regrouping. If we denote the transfer matrix between SS and S'S' as R_2, we have

$$R_2 = I \tag{2.11}$$

The transfer matrix between S'S' and $\bar{O}\bar{O}$ can be easily derived to be

$$R_3 = \begin{bmatrix} (2\sin\alpha-1)2\cos\beta & \rho/2\sin\beta & 0 & \rho(2\cos\beta-1)(1-2\cos\alpha)/2\cos\beta \\ -2\sin\beta/\rho & 0 & 0 & 2\sin\beta(2\cos\beta-1) \\ 0 & \rho(2\cos\beta-1) & 1 & \rho(3\beta-2\sin\alpha) \\ 0 & 0 & 0 & 1 \end{bmatrix} \tag{2.12}$$

The total matrix R(t) for the beam combiner system therefore is given by

$$R(t) = R_3 R_2 R_1 = R_3 R_1 \tag{2.13}$$

and can be shown to be given by

$$R(t) = \begin{bmatrix} -1 & \rho(2\cot\beta-3\operatorname{cosec}\alpha) & 0 & 0 \\ 0 & 1 & 0 & 0 \\ 0 & 0 & 1 & \rho(3\alpha-4\sin\alpha) \\ 0 & 0 & 0 & 1 \end{bmatrix} \tag{2.14}$$

We are now in a position to calculate the emittance growth in the beam combiner. From Eq. (2.14), we have

$$X_1 = R_{11} X_o + R_{12} X'_o \quad \text{and}$$

$$X_1' = X_o' \tag{2.15}$$

If x_o and x_o' are uncorrelated, the rms emittance is given by $[\ \langle x_o^2 \rangle \langle x_o'^2 \rangle\ ]^{1/2}$ before the beam combiner and by $[\ \langle x_1^2 \rangle \langle x_1'^2 \rangle\ ]^{1/2}$ after the beam combiner. We have

$$\langle x_1^2 \rangle \langle x_1'^2 \rangle = \langle x_o^2 \rangle \langle x_o'^2 \rangle \left[R_{11}^2 + R_{12}^2 \langle x_o'^2 \rangle / \langle x_o^2 \rangle \right] \tag{2.16}$$

The emittance growth factor therefore is given by

$$\left\{ R_{11}^2 + R_{12}^2 \langle x_o'^2 \rangle / \langle x_o^2 \rangle \right\}^{1/2}$$

$$= \left\{ 1 + R_{12}^2 \langle x_o'^2 \rangle / \langle x_o^2 \rangle \right\}^{1/2} \tag{2.17}$$

Figure 2.5 shows a plot of the emittance growth factor as a function of the bend angle α. In plotting Fig. 2.5, we have assumed that the radius of curvature to be 25 cm and took nominal values of x_o = 1 mm, x_o' = 1 mrad and $\Delta p/p$ = 1%.

The normalized electron brightness is given by

$$B = \frac{2I}{\gamma^2 \epsilon_x \epsilon_y} \quad \text{amp / m}^2\text{- stered} \tag{2.18}$$

The increase in pulse length is given by

$$R_{34} (\delta^2)^{1/2} \tag{2.19}$$

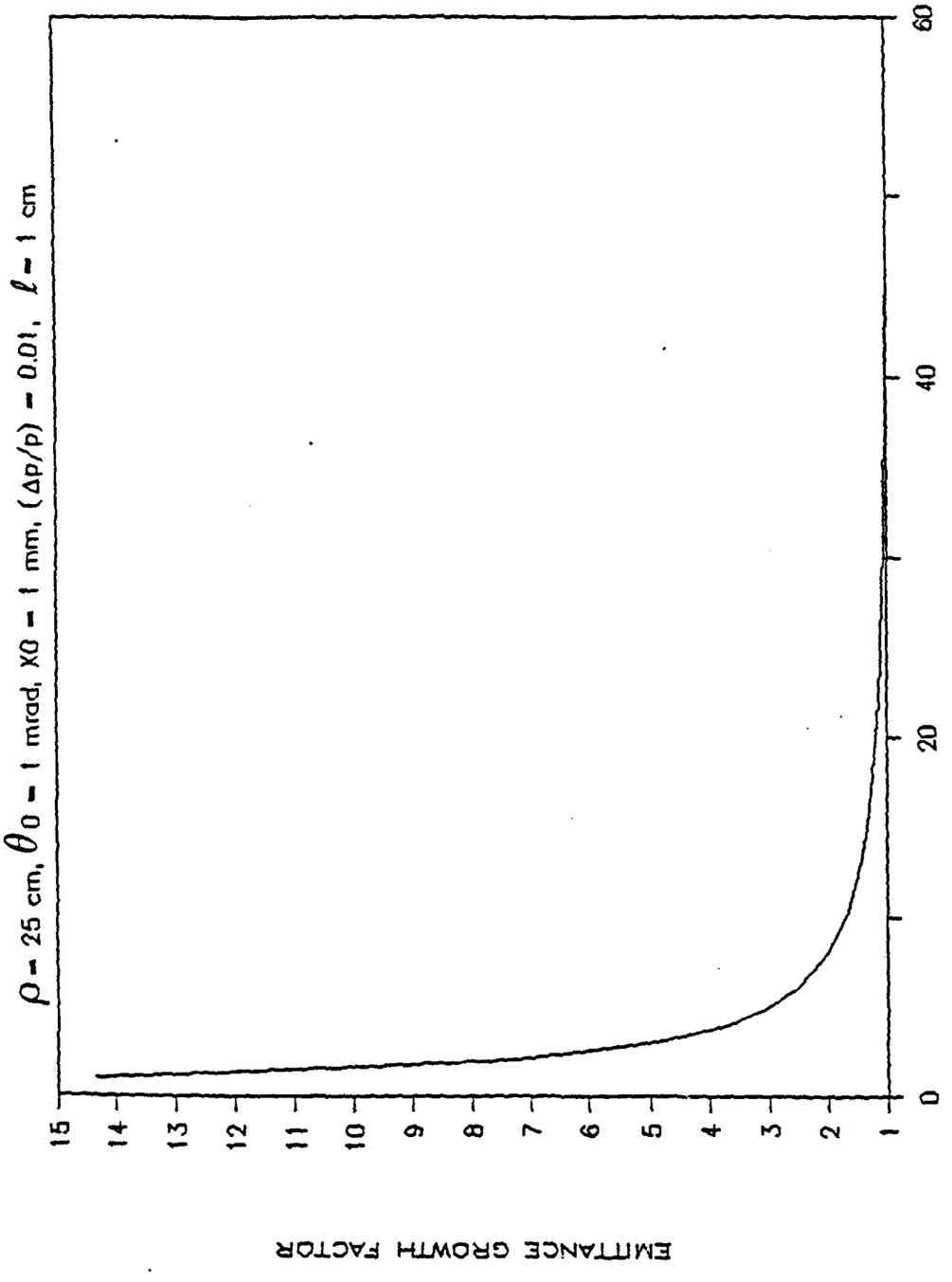

FIG. 2.5 - EMITTANCE GROWTH FACTOR VERSUS ALPHA

The peak current after the beam combiner is given by

$$I_p = 2\, I \quad ct_p \,/\, (ct_p + R_{34}\langle\delta^2\rangle^{1/2}) \tag{2.20}$$

where I is the peak current in each micropulse before the beam combiner. If we assume that ϵ_y does not change in the beam combiner, we can insert Eqs. (2.20) and (2.17) in Eq. (2.18) to obtain the brightness improvement as

$$\frac{2c\ t_p}{\{ct_p + R_{34}\langle\delta^2\rangle^{1/2}\}} \cdot \frac{1}{\{R_{11}^2 + R_{12}^2\ \langle x_o'^2\rangle \,/\, \langle x_o^2\rangle\ \}^{1/2}} \tag{2.21}$$

The pulse length increase is plotted in Fig. 2.6 where we have taken the initial pulse length to be ~33 psec (ℓ = 1cm). Figure 2.7 shows the brightness improvement as a function of the bend angle α. For $\alpha \lesssim 60^\circ$, we see an improvement of 80% in brightness.

If the bend angle is $\lesssim 8^\circ$, there is no brightness improvement. For bend angles between 30 and 40°, the brightness improvement is ~70%. If one takes into account second order effects and any misalignments or other aberrations, this increase in brightness may be lost.

We have shown that it is possible to increase the peak current and increase or maintain the beam brightness while doing this. In the next section we discuss how this affects FEL performance.

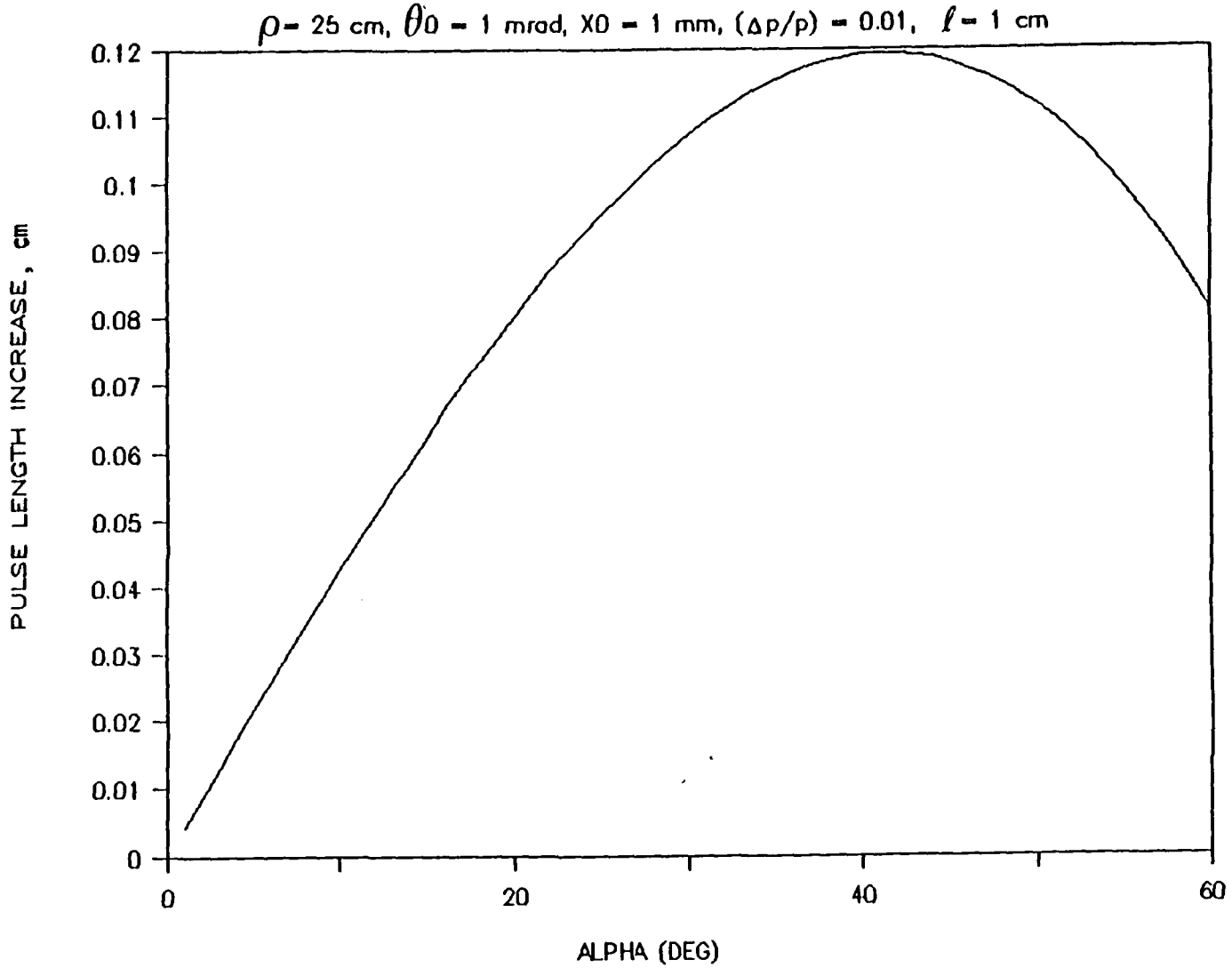

FIG. 2.6 - PULSE LENGTH INCREASE VERSUS ALPHA

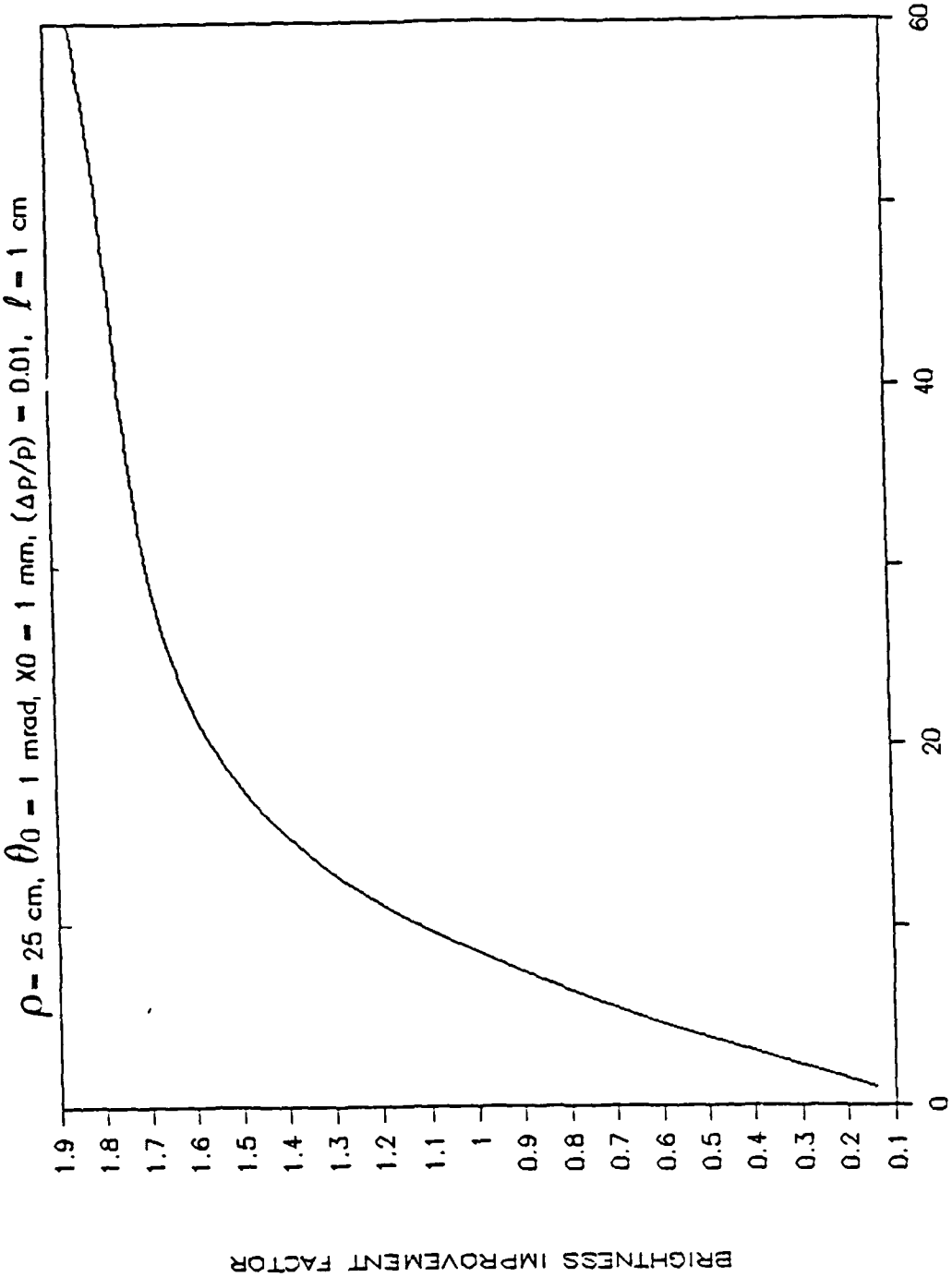

FIG. 2.7 - BRIGHTNESS IMPROVEMENT FACTOR VERSUS ALPHA

III. FEL PERFORMANCE ANALYSIS

In the free electron laser, the electrons are given a periodic transverse momentum through interaction with a periodic magnetic bending field or an a electromagnetic field traveling counter to the motion of the electrons. Kroll and McMullin[7] have shown that the effect of these two fields on the electron are equivalent. For simplicity, we shall consider the case of the relativistic electron beam moving inside a periodic magnetic field structure called the wiggler or the undulator. The magnetic field on axis can be either helical or planar sinusoidal. The radiation from the former will be circularly polarized while in the latter, it will be linearly polarized. For simplicity, we shall consider planar wiggler whose field or axis is specified by the vector potential

$$\vec{A}_w = \hat{x}\sqrt{2}\left(\frac{mc^2}{e}\right) a_w(z) \sin \int_0^z k_w(z')\, dz' \tag{3.1}$$

The radiation field propagating in the z-direction can be taken to be derived from the vector potential $\vec{A}_s$ given by

$$\vec{A}_s = \hat{x}\sqrt{2}\left(\frac{mc^2}{e}\right) a_s(z) \sin (k_s z - \omega_s t) \tag{3.2}$$

The quantities a_w and a_s are the dimensionless vector potentials. For magnetostatic wigglers, a_w is typically of the order of unity, while for radiation at a wavelength of 1 μm and a flux of 10^{10} w/cm^2, a_s is of the order of 10^{-4}. Thus, for practical parameters of interest, a_s can be neglected compared to a_w. We should point out that the assumption that A_w does not depend on transverse coordinates cannot be strictly satisfied, but if the

transverse dimensions of the electron beam are small, Eq. (3.1) is a reasonable approximation for field close to the axis of the wiggler. Later, we shall consider off-axis effects on the performance of the free electron laser.

The assumption that the vector potential $\vec{A}$ is independent of transverse coordinates implies that the transverse canonical momentum is a constant of the motion. The transverse velocity of the electron can therefore be written immediately as

$$\frac{\dot{x}}{c} = \beta_x = \sqrt{2}\,\frac{a_w}{\gamma}\,\sin\int k_w(z')\,dz' - \sqrt{2}\,\frac{a_w}{\gamma}\,\sin\,(k_s z - \omega_s t) \tag{3.3}$$

where we have assumed that the electron has no transverse velocity on entrance into the wiggler.

The energy equation is given by

$$\frac{d\gamma}{dt} = \frac{e}{mc}\,(\vec{\beta}.\vec{E}) \tag{3.4}$$

The electric field $\vec{E}$ can be obtained from Eq. (3.2) by straightforward differentiation. Using Eq. (3.3) for β_x we can write Eq. (3.4) as

$$\frac{d\gamma}{dt} = -\,\frac{\omega_s}{c}\,\frac{a_s a_w}{\gamma\beta_z}\left[\sin\psi + \sin\,(\psi - 2k_s z + 2\omega_s t)\right]$$

$$-\,\frac{\omega_s\,a_s^{\,2}}{c\;\;\gamma\beta_z}\,\sin\;\;(2\,k_s z\;\omega_s t)$$

where

$$\psi = \int_o^z k_w\,(z')\,dz' + k_s z - \omega_s t \tag{3.6}$$

The angle ψ denotes the phase of the transverse velocity of the electron relative to the radiation field. The evolution of ψ is obtained by differentiation of Eq. (3.6) as

$$\frac{d\psi}{dz} = k_w(z) + k_s - \frac{\omega_s}{c\beta_z} \tag{3.7}$$

If sin ψ in Eq. (3.5) is positive and quasi-stationary, the first term on the right hand side of Eq. (3.5) will contribute to the slowing down of the electron. The second and third terms are oscillating at about half the period of the wiggler and do not contribute to any significant net flow of energy between the electrons and the radiation field. For this reason, these terms are usually neglected. The condition when $\psi' = 0$ is called the resonance or syncronism condition. If we substitute $\omega_s = k_s c$ in Eq. (3.7), we obtain

$$\psi' = k_w - \frac{k_s}{2\gamma^2}(1 + a_w^2 - 2a_w a_s \cos\psi) \tag{3.8}$$

where we have used $\beta_z = 1$ whenever permissable and $(1 - \beta_z) = 1/2\gamma_z^2$. Setting $\psi' = 0$, the resonance condition is obtained as

$$k_s = 2\gamma^2 k_w(z)/(1 + a_w^2) \tag{3.9}$$

Thus, the motion of the electron in γ and ψ space is determined by the solution of Eq. (3.8) and

$$\gamma' = -\frac{k_s a_s a_w}{\gamma} \sin\psi. \tag{3.10}$$

The solution of Eqs. (3.8) and (3.10) for different initial conditions of ψ and γ_o, and averaging appropriately over these conditions will enable us to determine the performance of the free electron laser.

Along with the set of Eqs. (3.8) and (3.10) we have to solve the equations for the evolution of the optical field. If we let $k_s = k_{so} + \delta k_s$, it is easy to show that

$$\delta k_s = \frac{2\pi n e^2}{mc\omega_s} \frac{a_w}{a_s} \left[\overline{\frac{\cos \psi}{\gamma}}\right] \tag{3.11}$$

and

$$a_s' = \frac{2\pi n e^2}{mc\omega_s} a_w \left[\overline{\frac{\sin \psi}{\gamma}}\right] \tag{3.12}$$

where the bar denotes averaging over all the electrons.

Equations (3.8), (3.10), (3.11) and (3.12) are solved numerically with $k_w(z)$ and $a_w(z)$ being known input functions of z. For N electrons, Eqs. (3.8) and (3.10) really constitute a total of 2 N equations.

The effect of emittance on the performance of the FEL can be investigated by means of an effective energy spread. The energy spread is taken into account by taking an appropriate distribution of the initial conditions of the electrons.

The FEL has many physical parameters that can be varied; it is, therefore, impossible to make a complete parametric study of the performance of the FEL. To focus our problem on the effect of beam combining on the amplifier performance, we had to limit the independent parameters to only a few. A natural limitation is the length of the wiggler. Since the rf linac micropulse lengths are very short (≤30 psec), long wigglers are susceptible to the optical slippage problem. The electron beam slips behind the optical beam by one optical wavelength for every wiggler period traveled. If this slippage

amounts to >10% of the pulselength, it is clear that the electron beam tail would not contribute much to the generation of coherent light. Very long wiggler designs are based on the principle of optical guiding (refractive guiding) wherein the electron beam acts like a fiber and guides the optical beam through the wiggler preventing the diffraction expansion. To study the physics of optical guiding correctly, one has to solve the paraxial equation in three-dimensions. Since we are presenting only the results of a one-dimensional calculation, we did not want to invoke the optical guiding to increase the extraction efficiency. Accordingly, we restricted the wiggler length to three times the Rayleigh length of the incident optical beam.

The second restriction that we have placed on our calculations is that the wiggler period be constant. While varying the taper of the wiggler, one can change λ_w, a_w or both. Current day designs have all opted to keep λ_w constant because of the ease of construction. a_w is varied by changing the gap between the pole pieces. In what follows, we have taken λ_w to be 4 cm and the optical wavelength to be 1 μm. The wiggler length is taken to be 20 m.

The magnetic vector potential (normalized a_w) is taken to vary as

$$a_w = a_{wo} \exp[-(\alpha z)^2] \tag{3.13}$$

over the length of the wiggler. This exponential form has the advantage that the wiggler is relatively untapered at the entrance (i.e., $z/L_w \ll 1$) while the taper is appreciable towards the end of the wiggler. This allows the small signal gain to build up very fast in the front section of the wiggler as well as for the adiabatic capture of as many electrons as possible in the ponderomotive potential well. The final resonant energy of the electrons is given by

$$\gamma_{Rf} = \left[\lambda_w\left\{1 + a_{wo}^2 \exp[-2(\alpha L)^2]\right\}/2\lambda_s\right]^{1/2} \tag{3.14}$$

while the resonant energy at wiggler entrance is

$$\gamma_{Ri} = \left[\lambda_w\left\{1 + a_{wo}^2\right\}/2\lambda_s\right]^{1/2} \tag{3.15}$$

The energy taper therefore can be written as $(\gamma_{Ri} - \gamma_{Rf})/\gamma_{Rf}$. This is usually expressed as a percentage. The smaller the value of α in Eq. (3.13), the smaller is the energy taper. For a given input optical flux, the intial trapping fraction increases with decreasing α while the deceleration efficiency increases with increasing α. The extraction efficiency, which is approximately the product of trapping fraction and the deceleration efficiency reaches a maximum for a particular value of α that depends on other e-beam, wiggler and optical parameters.

The two most important parametric studies that are relevant for this concept are the effects of peak current and energy spread on extraction efficiency and gain. Figure 3.1 shows a plot of the extraction efficiency as a fraction of αL for three different peak currents. From this figure, it is clear that for the taper function that we have chosen, the optimum value of αL is ~0.8 for peak current in the range indicated. Current rf linacs are capable of providing peak current of 400 to 500 amp with good brightness. For the beam combiner concept to work well, we would like the peak current to be in the kiloampere range. In the calculations presented above, we have assumed that the incident energy distribution is gaussian with a one sigma point of 0.5 percent. This represents a FWHM energy spread of approximately one percent. A 1 MeV spread imposed by the beam comnbiner at 20 MeV would correspond to one percent of energy spread at 100 MeV, which is close to the

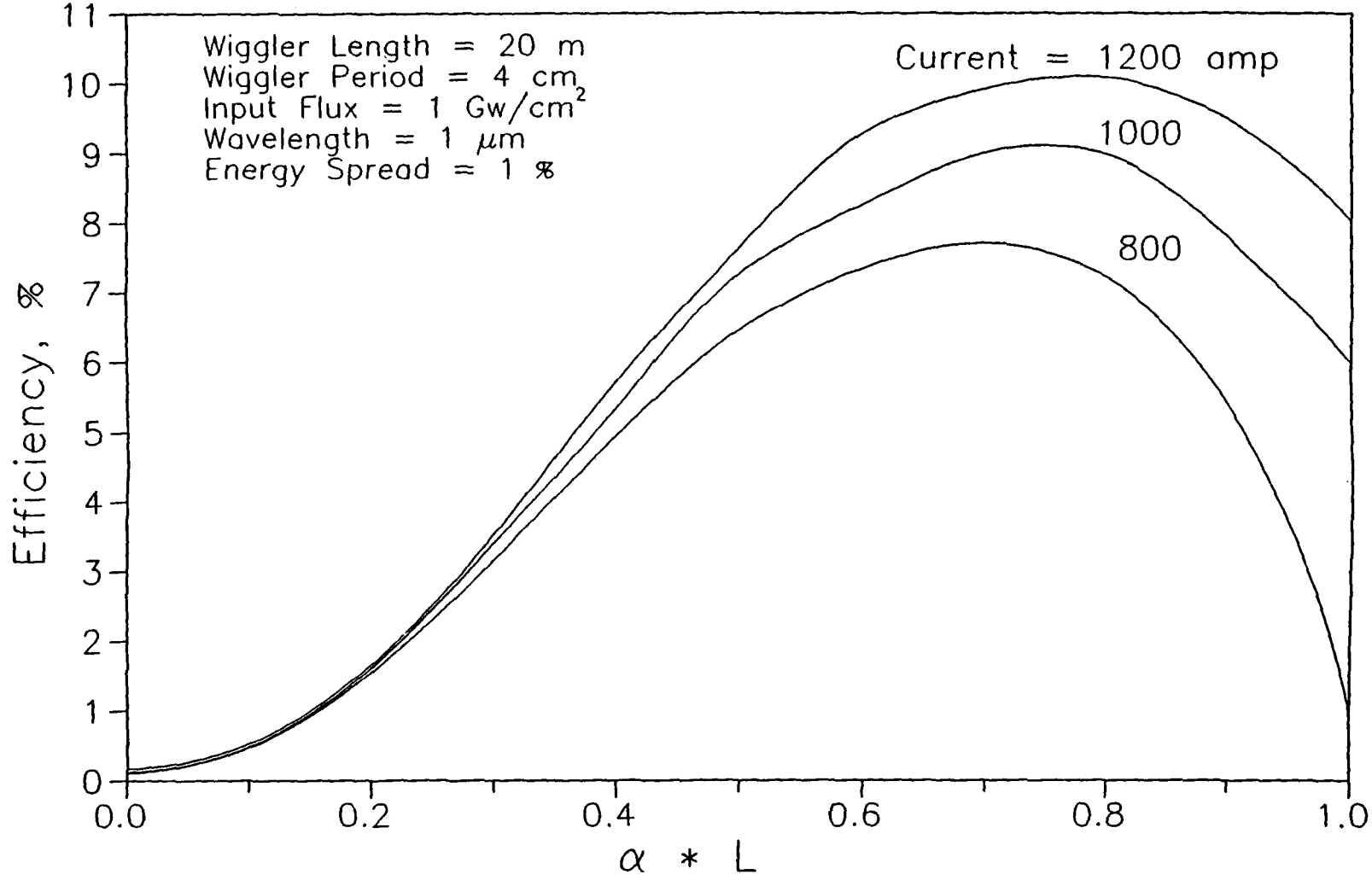

FIG. 3.1 - EFFECT OF WIGGLER TAPER ON EFFICIENCY

nominal energy for these calculations. Based on Fig. 3.1, we kept $\alpha L = 0.8$ while studying the effects of other parameters on the performance of the FEL amplifier. Excursions around this nominal value were also carried out.

Figure 3.2 shows a plot of the efficiency as a function of peak current for five different values of αL. As αL is increased, the current necessary to achieve a given extraction efficiency increases for low values of efficiencies. In the parameter range that we have investigated, we find that maximum efficiency is obtained for $\alpha L = 0.8$ for a peak current of 1200 amperes. What is interesting about Fig. 3.2 is that the shape of the curves resembles S, indicating a sudden increase in the extraction efficiency beyond a threshold value. For example, take the case of $\alpha L = 0.8$. Between 100 and 500 amperes, the efficiency increases linearly from 0.2 percent to 1 percent. The efficiency jumps from a value of ~1 percent at 500 amperes to ~4 percent at 600 amperes and ~7 percent at 700 amp. Beyond 700 amperes, the extraction efficiency still increases but the increase is less dramatic. The primary reason for attempting to increase the peak current is evident from this figure as the extraction efficiency increases faster than linearly beyond the threshold.

This increase in extraction efficiency, of course, comes at the expense of increasing the longitudinal phase space. It is therefore of some interest to find what the penalties are of increasing the energy spread in the beam. Figure 3.3 shows a plot of the extraction efficiency as a function of energy spread (FWHM). The total energy spread would be about twice of what is shown in the figure. The efficiency drops fairly linearly from a maximum for zero energy spread to almost zero for a value of $(\Delta\gamma/\gamma) \simeq 1.8\%$. As the peak current is increased, the value of $(\Delta\gamma/\gamma)$ at which a given extraction efficiency is reached increases indicating the utility as increasing the peak current. It is also clear from the figure that if the beam combiner operates

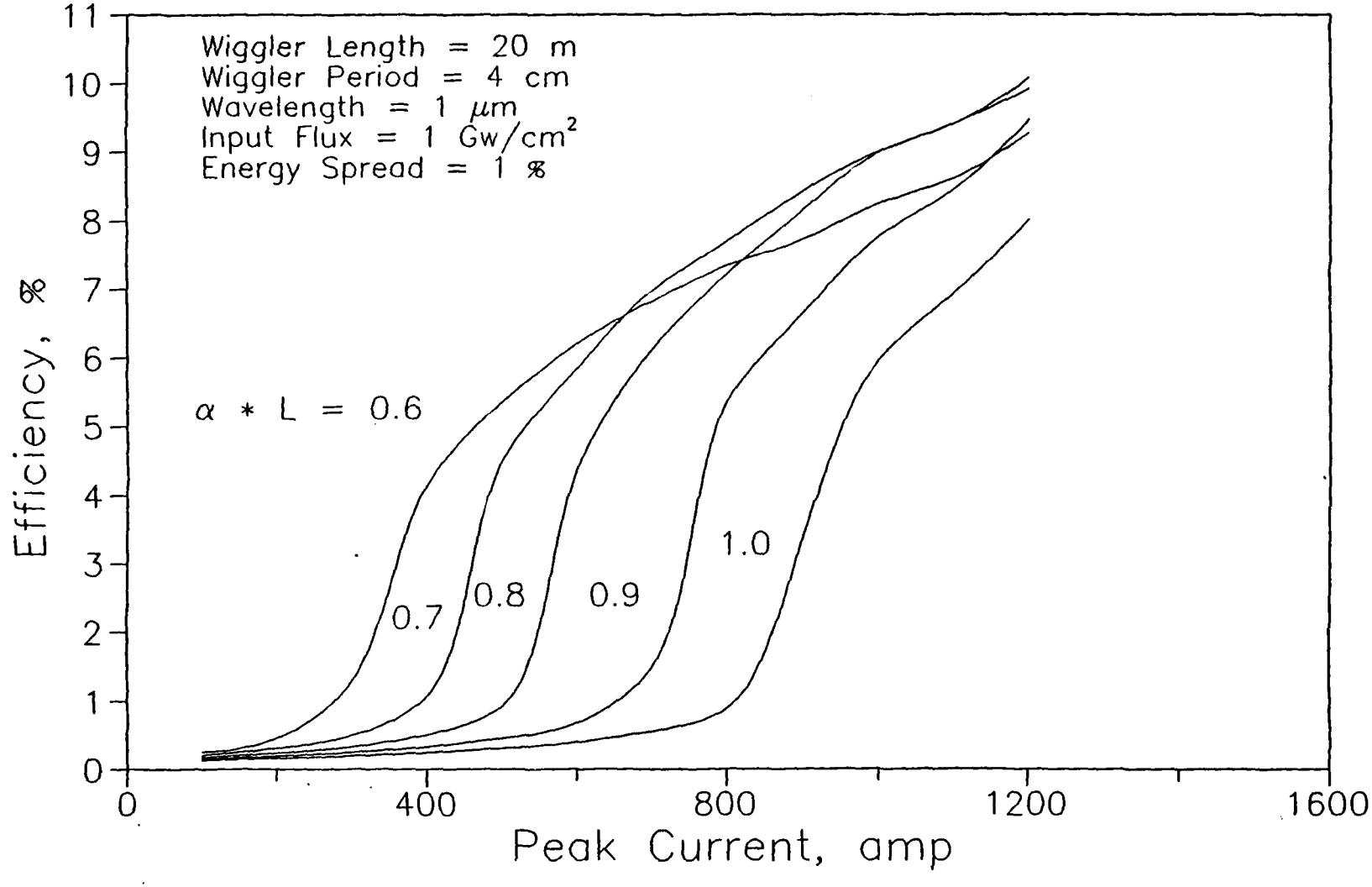

FIG. 3.2 - EFFICIENCY VERSUS PEAK CURRENT FOR DIFFERENT VALUES OF αL

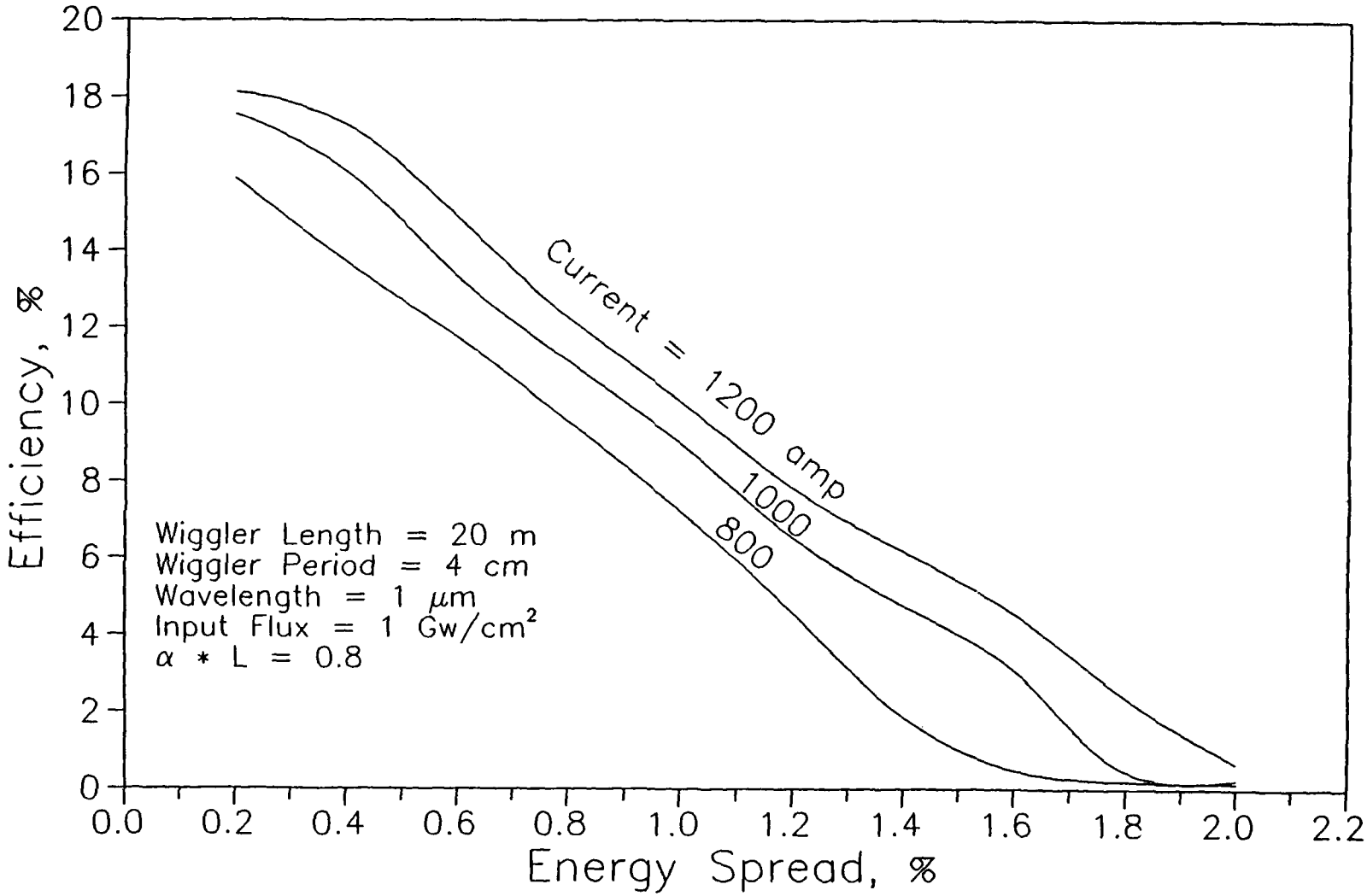

FIG. 3.3 - EFFECT OF ENERGY SPREAD ON EFFICIENCY

at a lower energy than the operating energy as the FEL, the net percentage energy spread is lower. Conventional linacs operating with micropulses spanning an angle θ of the rf wave have an energy spread $\simeq\theta^2/8$ due to the sinusoidal variation of the accelerating field. For θ = 0.2 rad, the energy spread would be ~0.5 percent. If the additional energy spread introduced by the beam combiner is of the same order as this or less, the loss in efficiency due to increased energy spread would be small compared to the increase in efficiency due to increased peak current.

Finally, the effect of input optical flux on the extraction efficiency was studied. Increasing the input flux from 1 to 10 Gw/cm^2 improves the extraction efficiency dramatically as can be seen from Fig. 3.4. Since we have taken the Rayleigh length to be one third of the wiggler length, a peak flux of 10 Gw/cm^2 corresponds to a power of $10^{10} \times \frac{20}{3} \times 10^{-6} \times 10^4 \simeq 700$ Mw. If the duty factor of the linac is $\approx 10^{-3}$, this would require an oscillator with less than 1 Mw average power. The peak output power would be in the range of 10 - 30 Gw giving a stage gain of 15 to 100 (12 to 20 dB) depending on the input power.

Our investigations show that a successful beam combiner can bring immense benefits to the operation of the FEL in a MOPA configuration. Longer wigglers that take advantage of the optical guiding can lead to much better wiggler designs and improved FEL performance. We did not invoke optical guiding because of the one-dimensional nature of our code. Our aim was to show that the beam combiner has many advantages in the operation of the FEL. Further analysis remains to be done to evaluate the MOPA designs and their performance thoroughly.

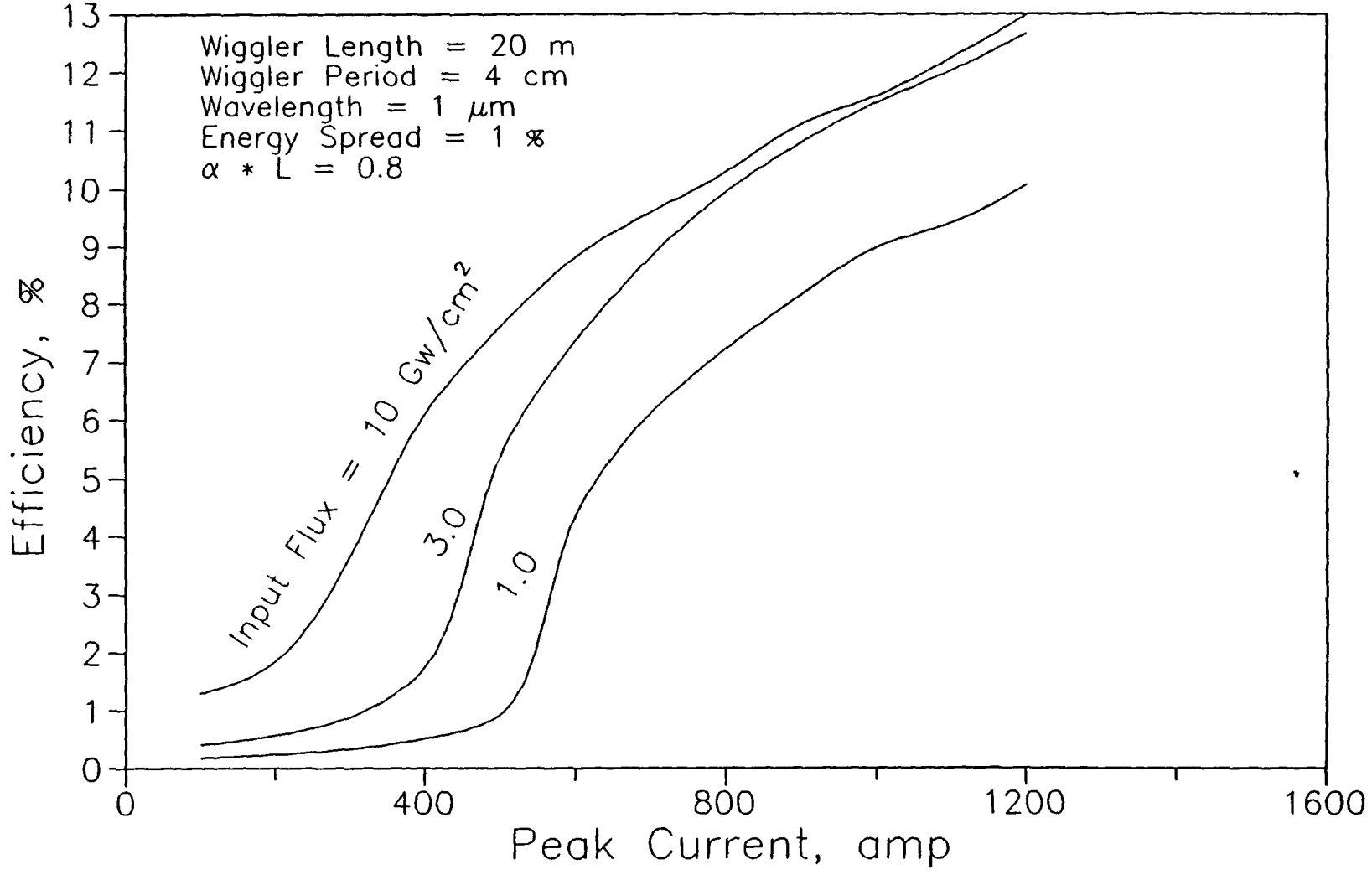

FIG. 3.4 - EFFICIENCY VERSUS PEAK CURRENT FOR DIFFERENT VALUES OF INPUT FLUX

IV. TRANSIENT STIMULATED RAMAN SCATTERING

In the downlink, the laser beam propagates from the mission mirror to the target which may be located 20 to 50 km above the ground at the time it is intercepted. Atmospheric absorption, thermal blooming and turbulence are not significant issues under these conditions. However, the Stimulated Rotational Raman Scattering (SRRS) in N_2 in the atmosphere imposes important constraints on the maximum amount of flux of coherent radiation that can be propagated through the atmosphere. The cross-section for the SRRS as a function of the wavelength of the incident radiation has been measured and theoretically calculated by several workers[8-10]. Using these values and using a simple model for the atmospheric density profiles, it is possible to obtain steady-state limits on the laser flux that can be transmitted through the atmosphere both in the uplink and in the downlink. The collisional dephasing time of the molecules increases with increasing altitude, and hence for pulsed lasers the Raman scattering during downlink is usually not in the steady-state regime but rather in the transient regime. The transient Raman gain is less than the steady-state Raman gain and it is of interest to find how the critical altitude (to which the propagation can take place in the downlink without significant Stokes conversion) varies as a function of the pulse length, wavelength, laser intensity and duty factor. In this section we describe how we have solved the transient Raman gain equations numerically for a train of pulses and have defined the critical altitude as a function of the average laser flux.

The pulse formats of the two leading free electron laser concepts are shown in Fig. 4.1. The individual pulses from the RFL/FEL are typically 20 to 30 psec long and are very short compared to the dephasing time in the molecules. However, the PRF in these lasers is rather high, being on the order of

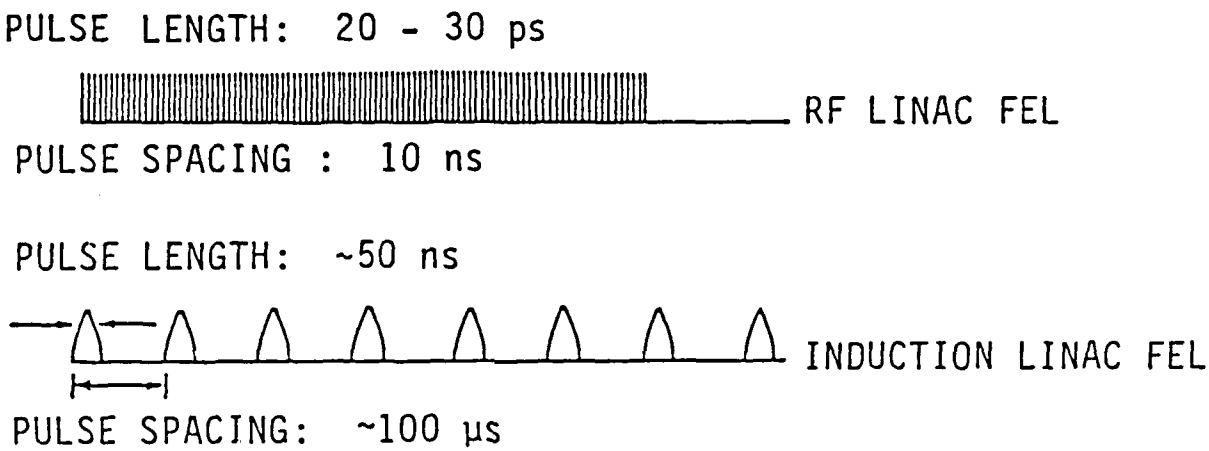

FIG. 4.1 - TYPICAL FEL WAVEFORMS

100 MHz. We, therefore, can expect the molecules to have memory of the passage of the previous pulses. This indeed proves to be the case. The quasi-steady state Raman gain for a train of pulses is higher than the maximum Raman gain for a single short pulse in the train. The IL/FEL pulse is typically ~50 nsec long and is somewhat in the transient regime. However, the interpulse time between successive IL/FEL pulses is ~100 μsec, which is long compared to the collisional dephasing time. Thus, the Raman scattering on each pulse takes place with practically no memory for the system regarding the propagation of earlier pulses through the medium.

The equations governing the transient stimulated Raman scattering can be written as[11]

$$(\partial/\partial z + \partial/v_1\partial t)E_1(t,z) = i(2\pi\omega_1^2/c^2k_1)NM_{fi}^*E_2A \tag{4.1}$$

$$(\partial/\partial z + \partial/v_2\partial t)E_2(t,z) = i(2\pi\omega_2^2/c^2k_2)NM_{fi}E_1A^* \tag{4.2}$$

$$[\partial/\partial t + \Gamma_{fi}(z)]A^*(t,z) = (i/\hbar)M_{fi}^*(\rho_i - \rho_f)E_1^*E_2 \tag{4.3}$$

with $|E_1|^2$ and $|E_2|^2$ being the intensities of the pump and Stokes fields, respectively; A is the material excitation; $N = N(z)$ is the number density of N_2; ρ_i and ρ_f are the probability densities of the initial and final states; $M_{fi} = \langle f|M|i\rangle$ is the Raman matrix element for the transition between $|i\rangle$ and $|f\rangle$ states; and $\Gamma_{fi}(z)$ is the dephasing rate. v_1 and v_2 are the group velocities at ω_1 and ω_2, and we can assume that $v_1 = v_2 = v$.

For the problem that we are trying to solve, we can assume that the depletion of the pump radiation as well as the induced population change are negligible. Then the above equations reduce to

$$(\partial/\partial z + \partial/v\partial t)E_2 = i\eta_1(z)E_1(t - z/v)A^* , \tag{4.4}$$

$$[\partial/\partial t + \Gamma(z)]A^* = -i\eta_2 E_1^*(t - z/v)E_2 , \tag{4.5}$$

where

$$\eta_1(z) = i(2\pi\omega_2^2/c^2k_2)N(z)M_{fi}$$

$$\eta_2 = M_{fi}^*(\rho_i - \rho_f)/\Gamma$$

We can simplify these further by the appropriate change of variables: let $T = t-z/v$ (retarded time) and $Z = z$, so that $\partial/\partial Z = \partial/\partial z+\partial/v\partial T$; also, let $E(T,Z) = E_2(T,Z)$, $F(T,Z) = i\eta_1 E_1(T)A^*(T,Z)$, $H(z) = \eta_1(Z)\eta_2$, and $P(T) = |E_2|^2\,\vartheta(T)$, where E_1 is a constant, and $\vartheta(T)$ is the step function. (It is not necessary to use a step function for E_1 in our procedure, but the computation time is significantly reduced if this is done, and the equations are somewhat simpler; for the problem that we are addressing, the actual pulse shape is insignificant.) Then our equations can be simplified to

$$\partial E/\partial Z = F(T,Z) \tag{4.6}$$

and

$$\partial F/\partial T = P(T)H(Z)E(T,Z)-\Gamma(Z)F(T,Z) \tag{4.7}$$

There exists an analytical solution of these equations for a uniform medium[11,12], in which H and Γ are constant. However, in the atmosphere, H and Γ are functions of altitude and could be complicated (especially if the temperature variations were taken into account), so that in general the analytical approach would fail. Several numerical procedures were considered and rejected by us as inefficient. Most prominent among them was using a conventional finite difference scheme on a two-dimensional grid to solve the equivalent hyperbolic equation. This method would require producing, storing, and inverting large ill-conditioned matrices, and if even at one point there would occur a numerical overflow, the whole inverted matrix would be incorrect (if the original one remained nonsingular). It would also require a much finer grid (more grid points) than the method we used. Alternatively, we could use a numerical two-dimensional integration procedure over rectangles or hexagons in the T-Z plane on the corresponding double-integral equation. This method would require too rigid and inconvenient relationships between the step sizes along the T and Z directions.

The approach that we took was based on the Adam-Bashforth type predictor-corrector method, which is conventionally used for ordinary differential equations. We have chosen the fifth order predictor and sixth order corrector formulas (we could "afford" such a high order, since the Adams-Bashforth type methods are relatively stable) that for an ODE $y' = f[x,y(x)]$ have the following form[13]:

$$y_{n+1} = y_n+(h/720)(1901y'_n-2774y'_{n-2}-1274y'_{n-3}+2511274y'_{n-4}) \qquad (4.8)$$

and

$$y_{n+1} = y_n+(h/1440)(475y'_{n+1}+1427y'_n-798y'_{n-1}+482y'_{n-2}-173y'_{n-3}+27y'_{n-4}) \qquad (4.9)$$

where h is the integration step size, and the subscripts refer to the points on the x-axis (separated by h), at which y' is evaluated and y is estimated. The main advantage of using a high order predictor-corrector method is in its high accuracy at low cost (since h can be chosen to be relatively large). The main disadvantages lie in the numerical instability for some equations and the necessity for some kind of single step method to initialize the multistep one. The accuracy of the single step method should be comparable to that of the multistep one; for example, the Runge-Kutta method is normally used to initialize the fourth order Adams-Moulton multistep one, since the local error in both of them is proportional to h^5. (In our method we cannot use a Runge-Kutta type starter, so we use a relatively complicated procedure, involving the Huen method and several increases of the step size.)

We start our calculations from the following initial and boundary conditions: $F(0,Z) = 0$, $E(0,Z) = E(T,0) = C$, where C is some positive constant that is chosen in such a way that makes a numerical overflow or underflow in the computations unlikely. Physically this means that we are starting the SRRS from a coherent seed, whose actual value is irrelevant to us, since we are only interested in the Raman gain, which equals $\ell n[E(T,Z)/E(T,0)] = \ell n[E(T,Z)/C]$. At first, F(T,0) is evaluated at the appropriate points from the analytical solution (which is easily obtained, since E(T,0) is a constant). Then we find F and E on the lines $(T,n\Delta Z)$ (n is an integer), line by line, until we span the region of interest in the T-Z plane. For any point lying well inside that region we proceed as follows: using the predictor formula with the values of $\partial F/\partial T$ at the previous five points for the same Z (we know them from before), we "predict" the value of F; then, using the corrector formula, with the value of F that we just found, as well as the values at the previous five points for the same T, we find the value of E at the current position. Using this value of E, we evaluate $\partial F/\partial T$,

and use it in the corrector formula for F; we repeat this process twice. Thus, we predict F once, correct it twice, and "correct" E three times (that is, use the corrector formula).

When the pump pulse ends, the E field departs from the region of interest with the speed of light, while the material excitation (and therefore F) decays due to collisions between the air molecules, so that the solution to our equations becomes: $E(T+\tau,Z) = F(T,Z)\exp(-\Gamma_c \tau)$, where γ is the duration of the first pulse, $\tau = T-T$, and Γ_c is the collisional frequency. Therefore, the initial conditions on F for the next pulse will depend on F(T) and time between the pulses. This variability is taken into account in our program. If a very long pulse needs to be considered, we can simply set the time between the pulses to zero (because the program has some memory limitations that set a limit on the single pulse duration).

The results of the program are the values of the total and the local gain $G_T(T,Z) = \ell n[E(T,Z)/E(T,0)]$ and $G_L(T,Z) = \partial(\ell nE)/\partial E = F(T,Z)/E(T,Z)$, which can later be plotted.

In order to test the performance of our program, we evaluated the analytical solution for the uniform medium case and compared it with the corresponding results obtained from the program. The agreement was to at least four significant figures, which exceeds the resolution of most computer-generated graphs. We also set the interpulse duration to zero and ran the program long enough to reach the steady-state limit in an exponential atmosphere. These results were compared with analytical results that one can obtain from Eqs. (4.6) and (4.7) by setting the time derivative in Eq. (4.7) to zero. Once again we found excellent agreement between the numerical results and analytical solutions verifying the stability and accuracy of the numerical procedure.

The transient Raman gain equations are solved to yield the exponential gain for a 'square hat' pump pulse as a function of the altitude and pump intensity. The propagation path in all downlink cases is assumed to be from space to the ground at an angle of 60° to the zenith. We assume that an intensity gain of e^{40} is required for almost complete conversion of the pump beam into the Stokes beam. The divergence angle of the Stokes beam is approximately given by D/L where D is the diameter of the beam and L is an effective gain length for Raman conversion. Typical values for D and L might be 0.3 m and 50 km, respectively. Thus, the converted Stokes radiation is still fairly well collimated. However, as this beam propagates downwards, the gain increases because of increasing N_2 number density down to ~45 km, below which point the gain is sensibly constant. The conversion from the first Stokes radiation into the second and higher order Stokes beams proceeds very rapidly. This process is illustrated in Fig. 4.2. Typical conversion lengths for these are 5 to 6 km. The higher order Stokes beams have therefore a much larger beam divergence angle than the first order beam; one can estimate the distance these beams would travel before their intensity drops by a factor of ~10. To take this physics into account in the downlink problem, we have calculated the altitude at which the gain becomes e^{40} and then subtracted 10 km from this altitude to obtain the critical altitude for propagation of the laser beam with a given intensity.

The calculations were carried out at the pump wavelength of 1.06 μm. The stimulated Raman gain scales almost linearly with the pump frequency in the wavelength region of 0.35 μm to 2.0 μm. It is therefore a simple matter to scale the intensity linearly with the wavelength to derive the results for wavelengths different than 1.06 μm. Figure 4.3 shows the critical altitude down to which the RFL/FEL pulses can propagate as a function of the duty factor for different average flux levels. The micropulse length for these

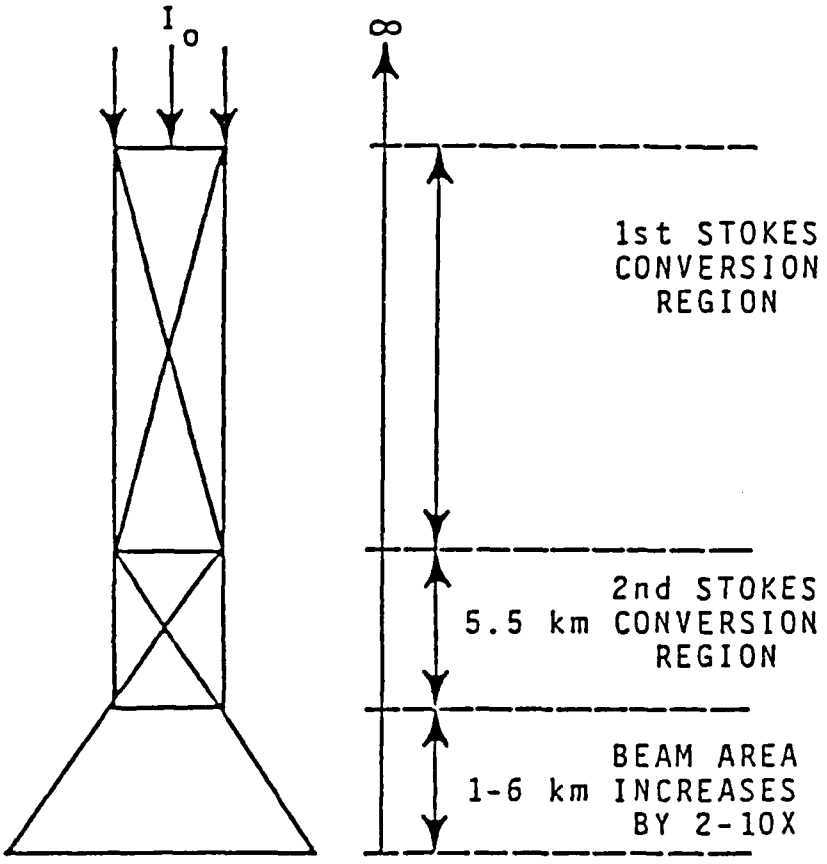

(U) • CALCULATE ALTITUDE AT WHICH FIRST STOKES GAIN IS EXP(40)

(U) • SUBTRACT ~ 10 km TO ALLOW FOR HIGHER ORDER STOKES CONVERSION AND BEAM AREA INCREASE

FIG. 4.2 - GEOMETRY FOR DETERMINING SRRS LIMIT ON DOWN LINK ALTITUDE

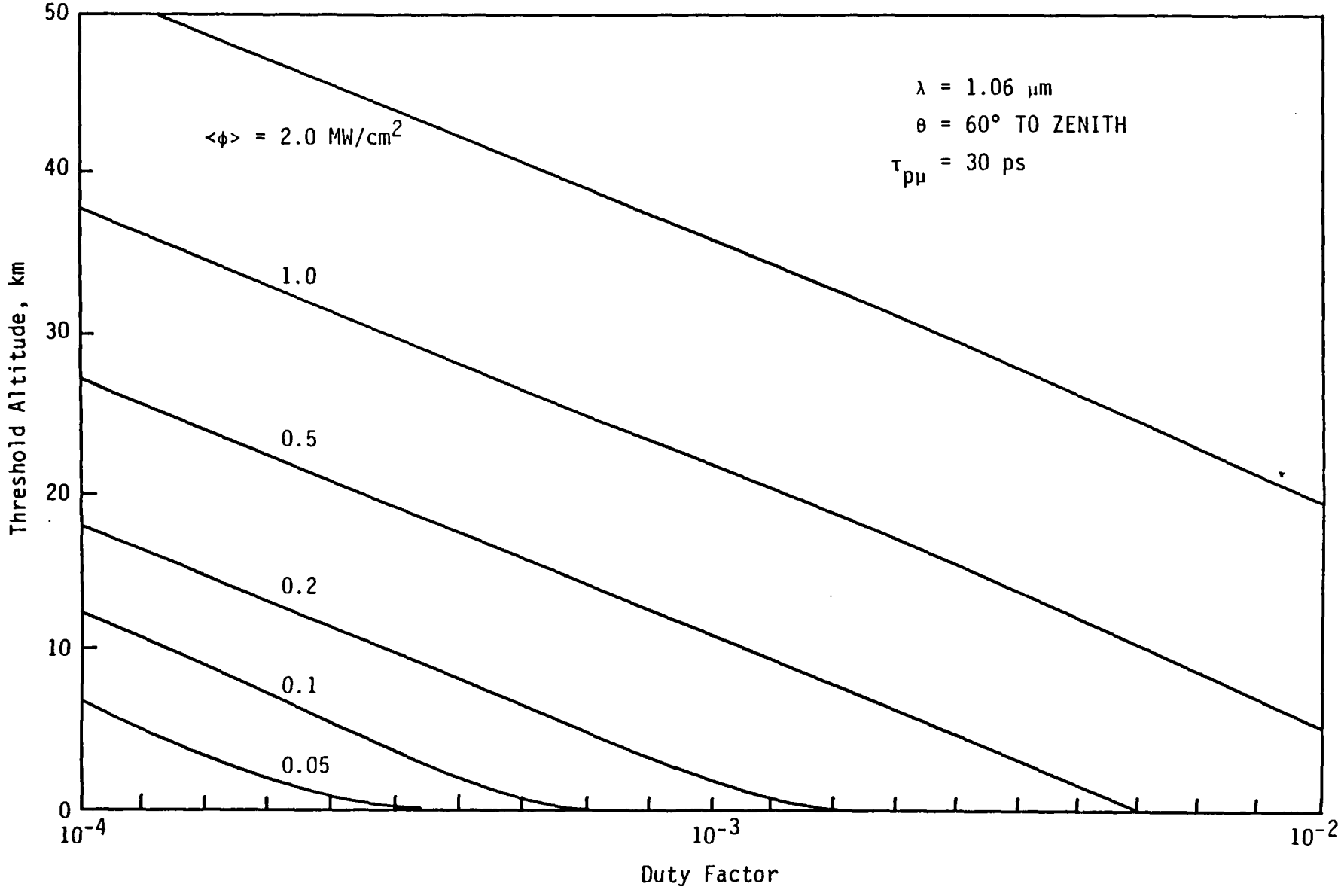

FIG. 4.3 - LIMITING ALTITUDE VERSUS DUTY FACTOR FOR RF LINAC FEL (PULSE LENGTH EQUALS 30 PS)

calculations was taken to be 30 psec which is typical for an accelerator working around 500 MHz. For the FELs of interest here, the duty factor is expected to be in the range of 1 to 3 x 10^{-3}. From the figure, it is clear that the RFL/FEL pulses will have no trouble getting down to ~10 km altitude with significant average fluxes. Figure 4.4 is similar to Fig. 4.3, except the micropulse length is set at 100 psec. In the latter case (i.e., Fig. 4.4), the Raman gain is higher, and for the same average flux and duty factor, the critical altitude is higher than that for the case of shorter micropulse length. The calculations show that the RFL pulses of pulse length less the 100 psec and duty factor $\geq$ 0.1% will have no trouble propagating down to ~10 km altitude at an average intensity of 0.3 MW/cm^2. Figure 4.5 shows the critical altitude as a function of peak intensity for a 50 nsec pulse and CW laser beam. A typical duty factor for the IL/FEL is ~ 5 x 10^{-4}. Under these conditions the minimum altitude down to which the pulse will propagate is about 50 km at flux levels of interest to SDI missions. There are two ways of bringing this altitude lower. The first one is to operate the IL/FEL at a lower peak power. The penalty one must pay for a lower peak power is the lower extraction and overall efficiency of the laser. The second workaround for the downlink SRRS problem is to use optical techniques to stretch the pulse length of the output beam, thereby reducing the peak power. Since the 50 nsec pulse has a lower Raman gain than a true CW beam, increasing the pulse length makes the Raman gain approach the CW gain limit more and more. A factor of 3 increase in pulse length does not change the results appreciably. To get significant decreases in the critical altitude, the pulse length has to be increased by at least a factor of 30.

In the uplink, the laser beam goes through dense air in the begining where the relaxation time is ~ 0.14 nsec. In this case the steady-state SRRS threshold is appropriate for the IL/FEL pulse lengths of 50 nsec, while the

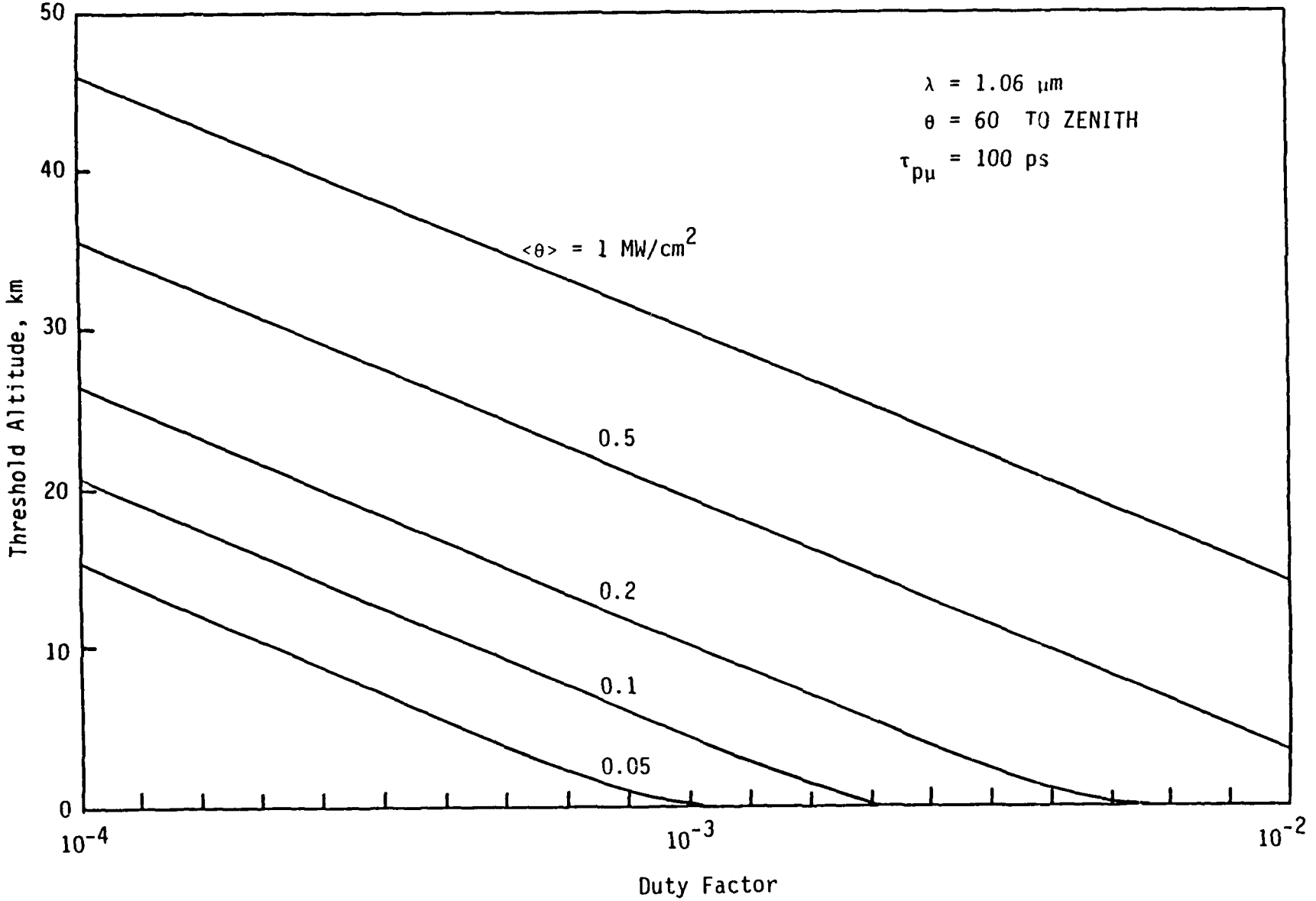

FIG. 4.4 - LIMITING ALTITUDE VERSUS DUTY FACTOR FOR RF LINAC FEL (PULSE LENGTH EQUALS 100 PS)

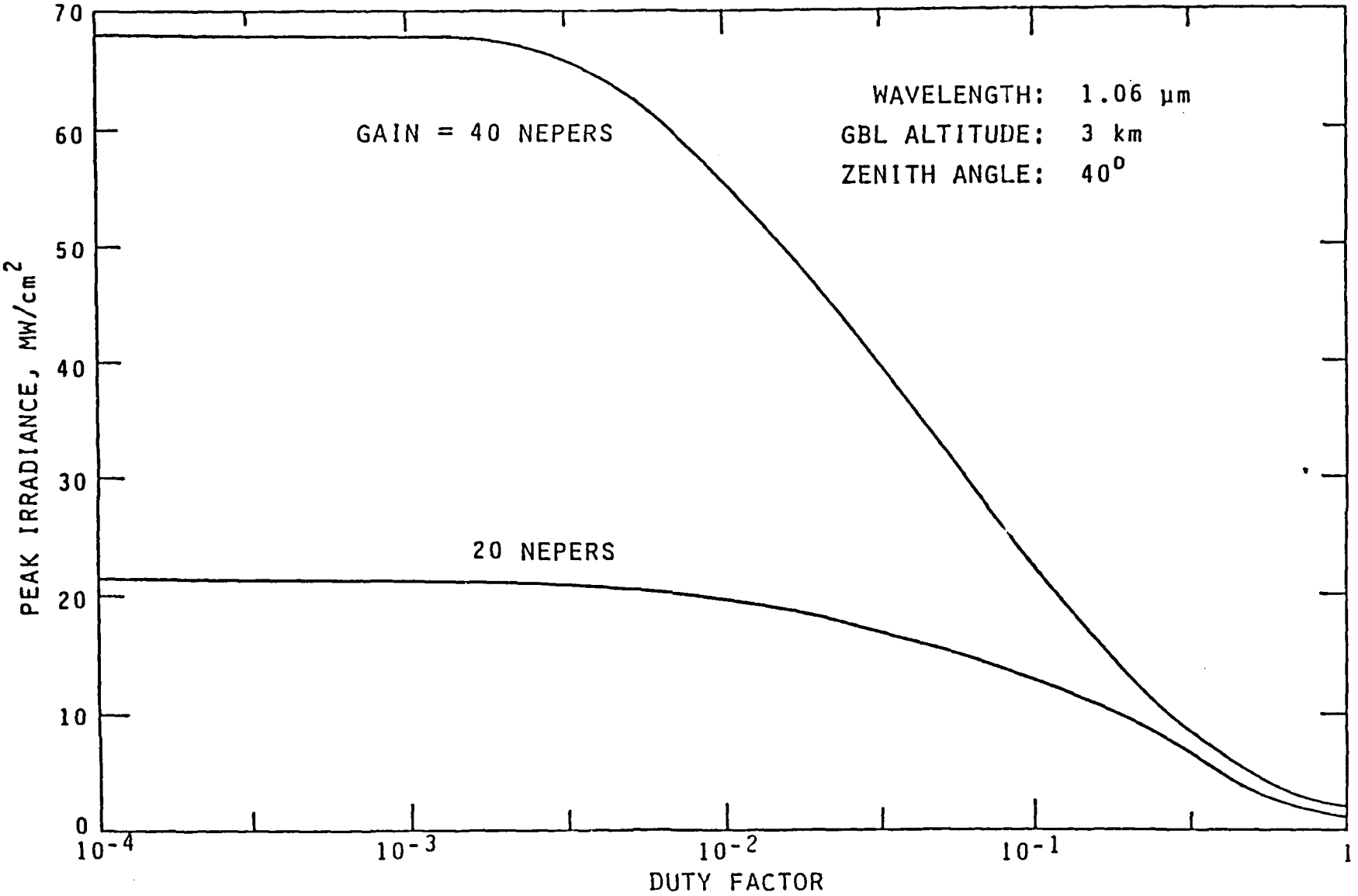

FIG. 4.5 - UPLINK SRRS IRRADIANCE LIMIT VERSUS DUTY FACTOR
(PULSE LENGTH EQUALS 30 PS)

much shorter pulse lengths (e.g., ≈ 30 psec) of the RFL/FEL can experience transient SRRS gain effects on the uplink propagation path. Thus, transient SRRS effects must be considered in specifying the minimum RFL/FEL aperture size.

Figure 4.6 shows the results of a transient SRRS analysis we have performed for uplink propagation at the 1.06 μm wavelength with a pulse length of 30 psec, which is typical of the RFL/FEL. The peak beam irradiances required to achieve uplink SRRS gains of 20 and 40 nepers, respectively, are plotted as functions of the duty factor in Fig. 4.6 for the case of a 3 km GBL altitude and 40° zenith angle. Operation at duty factors less than one with 30 psec pulses is shown to rapidly increase the threshold for significant SRRS conversion. (A gain of 40 nepers corresponds to that required for full conversion of the uplink beam to the first-stokes frequency, with the effective beam quality being seriously degraded as the beam exits from the top of the atmosphere layer; e.g., at ~ 50 km altitude.) For example, considering a 20 neper SRRS gain as an acceptable limit, allowing for the presence of sideband energy which may be present at the first stokes frequency in the RFL/FEL output spectrum, the threshold irradiance for 30 psec pulses is increased to about 20X the steady-state threshold value for duty factors of the laser less than 10^{-2}. Since 3×10^{-3} is typical for the RFL/FEL duty factor, based on present technology projections, the RFL/FEL would appear to have essentially no problems with uplink SRRS for any GBL power levels currently of interest.

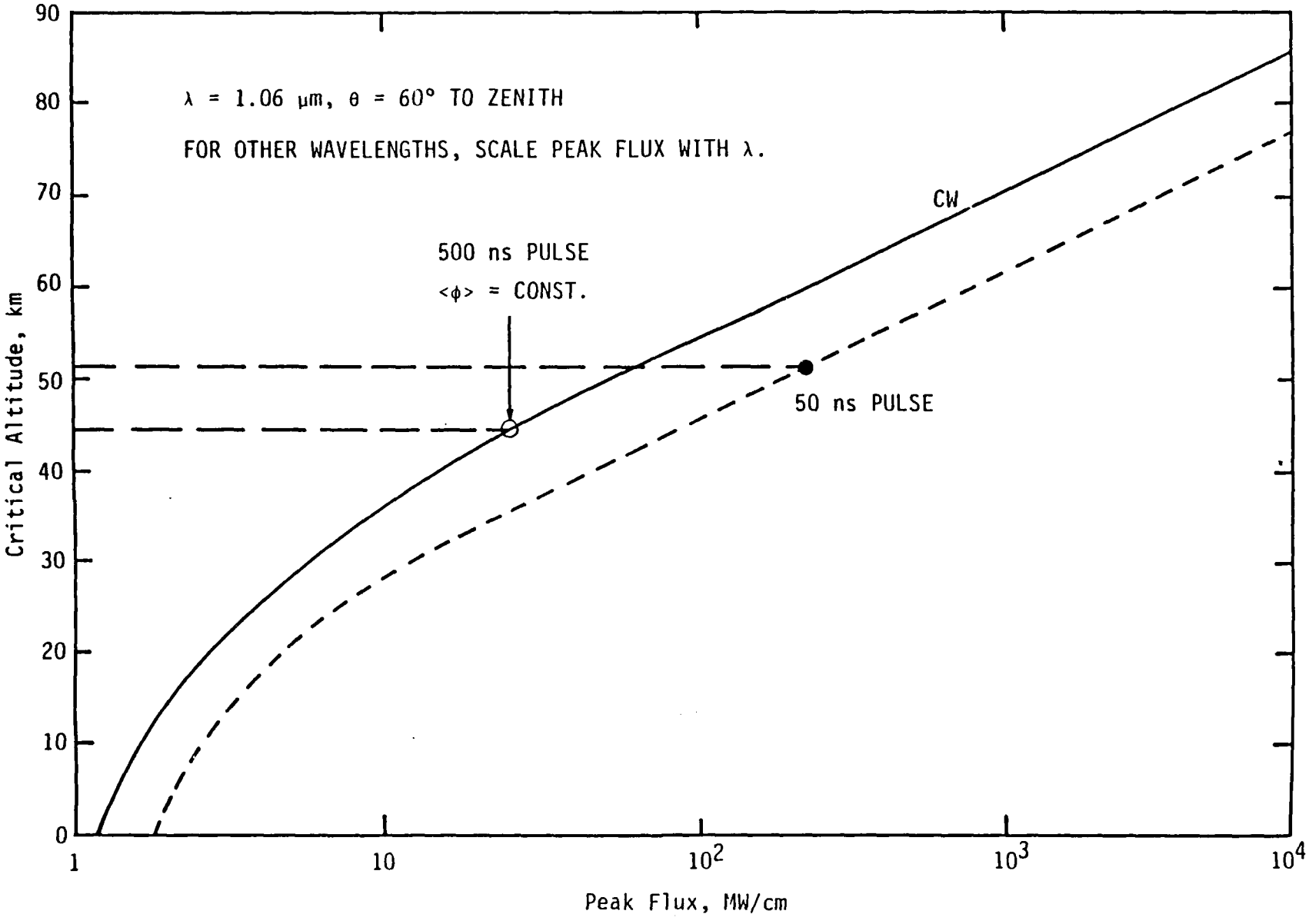

FIG. 4.6 - LIMITING ALTITUDE VERSUS PEAK FLUX FOR LONG PULSES

V. SUMMARY

We have shown in this report that the FEL performance can be markedly improved if the peak current can be increased to kiloampere level. These improvements can be obtained in relatively short wigglers (~20 to 25 m) without utilizing the optical guiding for increasing the extraction efficiency. Therefore, our results are somewhat conservative in this sense. Gains of 12 to 20 dB can also be realized concurrent with extraction efficiencies of > 8% in the amplifier.

We have analyzed on scheme for combining the electron micropulses to increase the peak current without degrading the beam brightness. The analysis was carried out to first order using matrix methods. The preliminary analysis was limited to one transverse direction only. The first order analysis clearly indicates the feasibility of the beam combiner concept. It requires further verification using TRANSPORT and TURTLE codes that are available. Even if the present concept is found to have drawbacks, it is always possible to have two accelerators that operate at, say, 20 and 21 MeV respectively and combine the micropulses from these two accelerators. The resulting micropulses can be further accelerated to 100 to 200 MeV required for the FEL MOPA operating in the visible or near IR. The effect of aberrations such as misalignment and manufacturing tolerance on the performance of the beam combiner have not been studied; nor have we included second and higher order effects. Hopefully, these will be studied in a future investigation.

We have also investigated the down link transient SRS problem through the atmosphere. The RF Linac FEL pulse format seems to be ideal in reducing the SRS growth rate through the atmosphere. For flux levels of interest to BMD, we do not foresee any problem in propagating the optical beam through the

atmosphere on the targets. In the uplink, thermal blooming is perceived to be the driver in determining the size of the optics and not SRS for power levels of interest in the BMD missions.

REFERENCES

1. S. Penner, *"Calculations of Properties of Magnetic Deflection Systems,"* in *Rev. Sci. Instr.*, 32, 150 (1961).
2. M. Herzberger, *"Modern Geometrical Optics,"* (Interscience Publishers, Inc., New York, 1958).
3. P.A. Sturrock, *"Static and Dynamic Electron Optics,"* (Cambridge University Press, New York, 1958).
4. E.D. Courant and H.S. Snyder, *Ann. Physics* 3, 1 (1958).
5. K.L. Brown, *"A First and Second-Order Matrix Theory for the Design of Beam Transport Systems and Charged Particle Sprectrometers,"* SLAC Report-75, Stanford Linear Accelerator Center, California (1982).
6. D.C. Carey, K.L. Brown, and Ch. Iselin, *"DECAY TURTLE,"* SLAC Report-246, Stanford Linear Accelerator Center, California (1982).
7. N.M. Kroll and W.A. McMullin, *Phys. Rev.* A17, 300 (1978).
8. M. Henesian, C. Swift, and J. Murray, *Opt. Lett.*, 10, 565 (1985).
9. M. Rokni and A. Flusberge, *I.E.E.E. J Quantum Electron.* QE-22, 1102 (1986).
10. G.C. Herring, W.K. Bischel, M.J. Dyer, and D.L. Huestis, *"Model for the Steady-state Rotational Stimulated Raman Gain Coefficients in the Atmosphere,"* SRI Technical Report No. MP 85-217, April 21, 1986.
11. Y.R. Shen, *The Principles of Nonlinear Optics* (John Wiley & Sons, New York, 1984), p. 177, 180.
12. C.S. Wang, *Phys. Rev.* 182, 482 (1969).
13. M. Klere, G.A. Korn, *Digital Computer User's Handbook* (McGraw-Hill, New York, 1967), p. 2-158.